

UNCLASSIFIED

AD NUMBER

ADB000487

LIMITATION CHANGES

TO:

Approved for public release; distribution is unlimited.

FROM:

Distribution authorized to U.S. Gov't. agencies only; Test and Evaluation; OCT 1974. Other requests shall be referred to Air Force Armament Laboratory, Attn: DLMA, Eglin AFB, FL 32542.

AUTHORITY

AFATL ltr, 10 Feb 1977

THIS PAGE IS UNCLASSIFIED

**THIS REPORT HAS BEEN DELIMITED
AND CLEARED FOR PUBLIC RELEASE
UNDER DOD DIRECTIVE 5200.20 AND
NO RESTRICTIONS ARE IMPOSED UPON
ITS USE AND DISCLOSURE.**

DISTRIBUTION STATEMENT A

**APPROVED FOR PUBLIC RELEASE;
DISTRIBUTION UNLIMITED.**

TECHNICAL REPORT AFATL-TR-74-168



**HIGH ALTITUDE SUPERSONIC TARGET
(HAST)**

F-4 GUIDANCE AND CONTROL SYSTEM ANALYSIS

**SYSTEMS ANALYSIS AND SIMULATION BRANCH
GUIDED WEAPONS DIVISION**

OCTOBER 1974



FINAL REPORT: December 1973 to June 1974

Distribution limited to U. S. Government agencies only; this report documents test and evaluation; distribution limitation applied October 1974. Other requests for this document must be referred to the Air Force Armament Laboratory (DLMA), Eglin Air Force Base, Florida 32542.

AIR FORCE ARMAMENT LABORATORY

AIR FORCE SYSTEMS COMMAND • UNITED STATES AIR FORCE

EGLIN AIR FORCE BASE, FLORIDA



AD B 000 487

UNCLASSIFIED

SECURITY CLASSIFICATION OF THIS PAGE (When Data Entered)

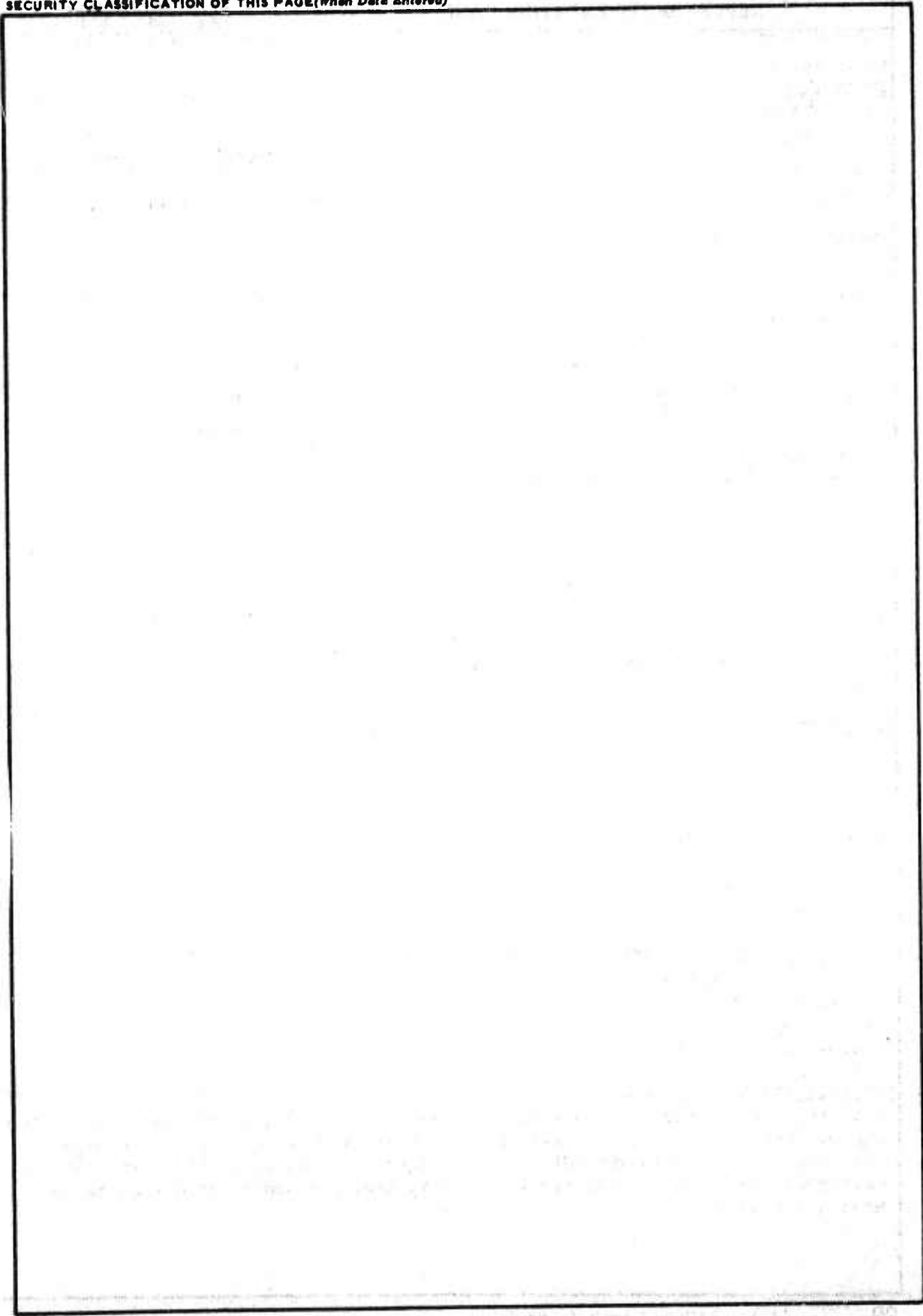
REPORT DOCUMENTATION PAGE		READ INSTRUCTIONS BEFORE COMPLETING FORM
1. REPORT NUMBER AFATL-TR-74-168	2. GOVT ACCESSION NO.	3. RECIPIENT'S CATALOG NUMBER
4. TITLE (and Subtitle) HIGH ALTITUDE SUPERSONIC TARGET (HAST) KJ-4 GUIDANCE AND CONTROL SYSTEM ANALYSIS		5. TYPE OF REPORT & PERIOD COVERED Final Report December 1973 - June 1974
7. AUTHOR(s) Matthew D. Rezmer		6. PERFORMING ORG. REPORT NUMBER
9. PERFORMING ORGANIZATION NAME AND ADDRESS Guided Weapons Division (DLMA) Air Force Armament Laboratory Eglin Air Force Base, Florida 32542		8. CONTRACT OR GRANT NUMBER(s)
11. CONTROLLING OFFICE NAME AND ADDRESS Air Force Armament Laboratory Air Force Systems Command Eglin Air Force Base, Florida 32542		10. PROGRAM ELEMENT, PROJECT, TASK AREA & WORK UNIT NUMBERS Project 469A0101
14. MONITORING AGENCY NAME & ADDRESS (if different from Controlling Office)		12. REPORT DATE October 1974
		13. NUMBER OF PAGES 61
		15. SECURITY CLASS. (of this report) UNCLASSIFIED
		15a. DECLASSIFICATION/DOWNGRADING SCHEDULE
16. DISTRIBUTION STATEMENT (of this Report) Distribution limited to U. S. Government agencies only; this report documents test and evaluation; distribution limitation applied October 1974. Other requests for this document must be referred to the Air Force Armament Laboratory (DLMA), Eglin Air Force Base, Florida 32542.		
17. DISTRIBUTION STATEMENT (of the abstract entered in Block 20, if different from Report)		
18. SUPPLEMENTARY NOTES Available in DDC.		
19. KEY WORDS (Continue on reverse side if necessary and identify by block number) High Altitude Supersonic Target Guidance and Control System System Analyses Flight Test Mission		
20. ABSTRACT (Continue on reverse side if necessary and identify by block number) This technical report presents the results of preflight, postflight, and system improvement guidance and control analyses performed in support of the High Altitude Supersonic Target (HAST) KJ-4 flight test mission. The work that was performed consisted of analytical stability analyses and related simulation analysis studies.		

DD FORM 1 JAN 73 1473 EDITION OF 1 NOV 65 IS OBSOLETE

UNCLASSIFIED
SECURITY CLASSIFICATION OF THIS PAGE (When Data Entered)

UNCLASSIFIED

SECURITY CLASSIFICATION OF THIS PAGE(When Data Entered)



UNCLASSIFIED

SECURITY CLASSIFICATION OF THIS PAGE(When Data Entered)

PREFACE

The analytical studies discussed in this technical report were accomplished in support of Project 469A0101 at the Air Force Armament Laboratory between December 1973 and June 1974. Mr P. Pietrzak (AFFDL/FGD, Wright-Patterson Air Force Base) and Mr S. Rosengarten (4950th TESTW/ADS, Wright-Patterson Air Force Base) provided valuable assistance during the hybrid simulation analysis studies.

This technical report has been reviewed and is approved for publication.



RICHARD M. KELLER, Colonel, USAF
Chief, Guided Weapons Division

TABLE OF CONTENTS

Section		Page
I	INTRODUCTION	5
II	PREFLIGHT ANALYSIS	8
	1. Stability Analysis	8
	2. Simulation Analysis	27
III	FLIGHT TEST RESULTS	29
IV	POSTFLIGHT ANALYSIS	40
	1. Data Analysis	40
	2. Simulation Analysis	40
V	SYSTEM IMPROVEMENTS	47
VI	CONCLUSION AND RECOMMENDATIONS	58

SECTION I

INTRODUCTION

The objective of the High Altitude Supersonic Target (HAST) KJ-4 guidance and control system analysis study was initiated to provide preflight and postflight analysis support through the flight test mission and to identify system performance improvement. These objectives were met through analytical stability studies, flight test data evaluation, and simulation analysis of the system. The following paragraphs chronologically list and summarize these analyses.

The preflight stability analysis objectives were to determine the stability characteristics (gain and phase margin), response characteristics (loop and system frequencies), and anticipated performance of the guidance and control system. This was achieved by performing a root locus stability analysis of discrete flight conditions, as defined by the flight test trajectory, and by evaluating the resultant plots. The stability analysis investigated the basic longitudinal and lateral airframe stability, individual autopilot loop stability, and overall system stability. The stability analysis determined the system to be stable, responsive, and able to meet the proposed flight test requirements.

Next, simulation analysis studies were performed to dynamically evaluate the previous stability analysis, determine system sensitivity requirements, and define the overall system performance. These studies were accomplished utilizing six-degrees-of-freedom hybrid and digital simulation programs at Wright-Patterson Air Force Base and at the Air Force Armament Laboratory. The simulation analysis of the stability study evaluated the longitudinal and lateral airframe responses, individual loop response, and overall system response. The results were identical and, thus, verified the stability analysis and simulation modeling of the system. The system sensitivity and performance analysis was conducted next and investigated the effects of launch transients, autopilot gain variations, thrust misalignment, wind shears and gusts, canard and aileron actuator rate variations, differentiator noise, and variation of programmed maneuvers. The previous stimuli were applied individually and in combination for nominal and excessive values. The simulation analysis dynamically concluded the system to be stable, responsive, and able to meet the proposed flight test requirements.

The flight test of KJ-4 took place on 22 March 1974 with the following results. Although the guidance and control system was operational and functioned properly throughout the initial 10 seconds of flight, the system was unable to maintain stable flight in the longitudinal plane. A divergent oscillation was present from launch, and this eventually saturated the control effectiveness and resulted in an uncontrolled and unstable flight.

In addition, an aileron actuator failure was observed to have occurred approximately 11 seconds into the flight when the system was beyond control. An initial evaluation of real time telemetry data showed that the indicated altitude differed from the true radar altitude measurements. A further evaluation disclosed that the indicated altitude measurements were sensitive to angle-of-attack variations, and this sensitivity produced a destabilizing altitude error of approximately 100 feet per degree of angle-of-attack. This error was properly processed by the autopilot, but its magnitude exceeded the longitudinal guidance and control system performance capabilities.

Postflight simulation analysis studies were performed next in order to evaluate the results of the flight test data analysis. The simulation analysis duplicated the flight test results when the simulation model included the previously described altitude error. This verified the simulation analysis model. After the altitude error had been defined and modeled and duplicate results were obtained, a stability analysis was initiated to evaluate the guidance and control stability characteristics for recommendation of system improvements.

Follow-on stability and simulation analysis concentrated on the KJ-4 autopilot mechanization and on the effects that altitude error had on the stability characteristics of the system. The results of the analysis showed that an error of 10 feet per degree of angle of attack would be required for stable flight. The initial indications were that this was beyond the capabilities of the current altimeter sensor, and emphasis would be placed on altitude error reduction and investigation of alternate autopilot mechanizations. The various candidate mechanizations, which were defined through analysis, represent increasingly more complex systems with resultant increased performance capabilities. Beyond the present autopilot configuration, these mechanizations would be:

- a. Integral of accelerometer.
- b. Pitch attitude.
- c. Double integration of accelerometer.
- d. Derived angle of attack.
- e. Autopilot signal shaping.
- f. An adaptive (gain scheduling) autopilot.

Proper selection of a previous mechanization is contingent on wind tunnel testing being performed on the altitude sensor and on the resultant definition of the altitude error throughout the performance envelope. For the mechanization selected, an extensive stability and simulation analysis will be performed to investigate the system performance throughout the flight envelope.

The altitude error observed during the KJ-4 flight test is a dynamic error that can only be determined through dynamic flight test or during separate wind tunnel tests for investigating this anomaly. Although the flight test mission objectives were not totally satisfied, crucial data were obtained, and solutions to the problems encountered have been identified and are undergoing further refinement.

SECTION II

PREFLIGHT ANALYSIS

1. STABILITY ANALYSIS

The preflight stability analysis was performed to investigate the guidance and control system stability and performance characteristics. The system gain and phase margins, operating frequencies, and time constants typify the characteristics determined by this analysis. The analysis was accomplished through root locus analysis of the system longitudinal and lateral autopilots for discrete flight conditions contained within the KJ-4 flight test trajectory. Specifically, discrete missile airframe dynamic responses were defined, and the resultant transfer functions were then substituted into the system block diagram for root locus analysis investigation. The root locus analysis investigated the innermost autopilot loop initially and proceeded to obtain the resultant plots and closed loop response required for closure of the next autopilot loop. This process was repeated until the complete system was analyzed. Evaluation of the resultant root locus plots defined the individual loop and the complete system stability characteristics. Correlation of the results obtained, for the discrete cases investigated, allows determination of the overall system stability characteristics throughout the flight test trajectory. Table 1 summarizes the results of the analysis, and the following paragraphs provide a detailed discussion of the procedure followed.

The KJ-4 flight test mission was defined by the following conditions: launch Mach = 1.5 and launch altitude = 50,000 feet, cruise Mach = 2.0 and cruise altitude = 50,000 feet. From the previous mission conditions, discrete missile airframe dynamic responses were selected as representative of flight test performance. Table 2 states the resultant longitudinal and lateral airframe transfer functions that were used for the ensuing analysis. These transfer functions were then substituted into the longitudinal and lateral autopilot block diagrams presented in Figures 1 and 2, and an analysis was performed for each dynamic case.

The longitudinal autopilot has two modes of operation and a specific functional configuration for each. Under normal operation, the longitudinal autopilot consists of the pitch rate damping loop, altitude rate damping loop, and altitude guidance loop. Specifically, the rate damping loop provides stability augmentation to the airframe and increased short period performance capabilities. The altitude rate damping loop is used for providing lead information to the outer altitude guidance loop and for altitude damping. The altitude guidance loop function is to provide stable and level flight throughout the flight profile. In performing g maneuvers, the longitudinal autopilot configuration is modified by the removal of the altitude guidance loop and by the activation of an acceleration loop. The acceleration loop provides damping and lead information to the altitude rate guidance loop, and the altitude rate loop is used in place of the altitude position loop for maintaining stable and level flight.

TABLE 1. PREFLIGHT STABILITY ANALYSIS SUMMARY

Analysis Cases	Natural Frequency (rad/sec)	Gain Margin (% of nominal)	Phase Margin (degrees)
<u>Longitudinal Autopilot</u>			
Rate damping loop - Case 1	2.5	>+ 20	>20
Rate damping loop - Case 2	2.7	>+ 20	>20
Altitude rate loop - Case 1	0.2	>+ 20	>20
Altitude rate loop - Case 2	0.5	>+ 20	>20
Altitude loop - Case 1	0.1	>+ 20	>20
Altitude loop - Case 2	0.5	>+ 20	8
Acceleration loop - Case 1	0.8	>+ 20	18
Acceleration loop - Case 2	1.4	>+ 20	7
Altitude rate loop (closed through acceleration) - Case 1	0.7	>+ 20	10
Altitude rate loop (closed through acceleration) - Case 2	0.8	+ 10	3
<u>Lateral Autopilot</u>			
Rate damping loop - Case 2	1.5	>+ 20	>20
Roll attitude loop - Case 2	1.0	>+ 20	>20
Yaw attitude loop - Case 2	0.1	+ 10	3

TABLE 2. AIRFRAME TRANSFER FUNCTIONS^a

Longitudinal Transfer Functions

Case 1. Mach = 1.2 weight = 1040 lb Case 2. Mach = 2.0 weight = 966 lb
 h = 50,000 ft α = 6.8 degrees h = 55,000 ft α = 3.7 degrees

$$\frac{\dot{\theta}}{\delta_1} = \frac{19.95 (S + 0.22)}{(S^2 + 0.96S + 24.1)} \equiv (\Delta\theta_1)$$

$$\frac{\dot{\gamma}}{\delta_1} = \frac{4.33}{(\Delta\theta_1)}$$

$$\frac{\alpha}{\delta_1} = \frac{19.95}{(\Delta\theta_1)}$$

$$\frac{\dot{\gamma}}{\dot{\theta}_2} = \frac{\dot{\gamma}}{\delta_1} \cdot \frac{\delta_1}{\dot{\theta}} = \frac{0.217}{(S = 0.22)}$$

$$\frac{\dot{\theta}}{\delta_2} = \frac{32(S + 0.23)}{(S^2 + 1.02S + 43.3)} \equiv (\Delta\theta_2)$$

$$\frac{\dot{\gamma}}{\delta_2} = \frac{7.5}{(\Delta\theta_2)}$$

$$\frac{\alpha}{\delta_2} = \frac{32.0}{(\Delta\theta_2)}$$

$$\frac{\dot{\gamma}}{\dot{\theta}_2} = \frac{\dot{\gamma}}{\delta_2} \cdot \frac{\delta_2}{\dot{\theta}} = \frac{0.234}{(S + 0.23)}$$

Lateral Transfer Functions

Case 2. Mach = 2.0 weight = 966 lb
 h = 55,000 ft α = 3.7

$$\frac{\dot{\beta}}{\delta_2} = \frac{(2.29) (S + 0.345) (S + 0.253)}{(S + 0.056) (S + 0.303) (S^2 + 0.4S + 56.3)} \equiv (\Delta\phi_2)$$

$$\frac{\dot{\phi}}{\delta_2} = \frac{(34.9) (S) (S^2 + 0.5S + 49)}{(\Delta\phi_2)}$$

$$\frac{\dot{\psi}}{\delta_2} = \frac{(-0.005) (S + 0.26) (S - 93.1) (S + 239.4)}{(\Delta\phi_2)}$$

$$\frac{\psi}{\dot{\phi}_2} = \frac{\psi}{\delta_2} \cdot \frac{\delta_2}{\dot{\phi}} = \frac{(-0.005) (S + 0.26) (S - 93.1) (S + 239.4)}{(34.9) (S) (S^2 + 0.5S + 49)}$$

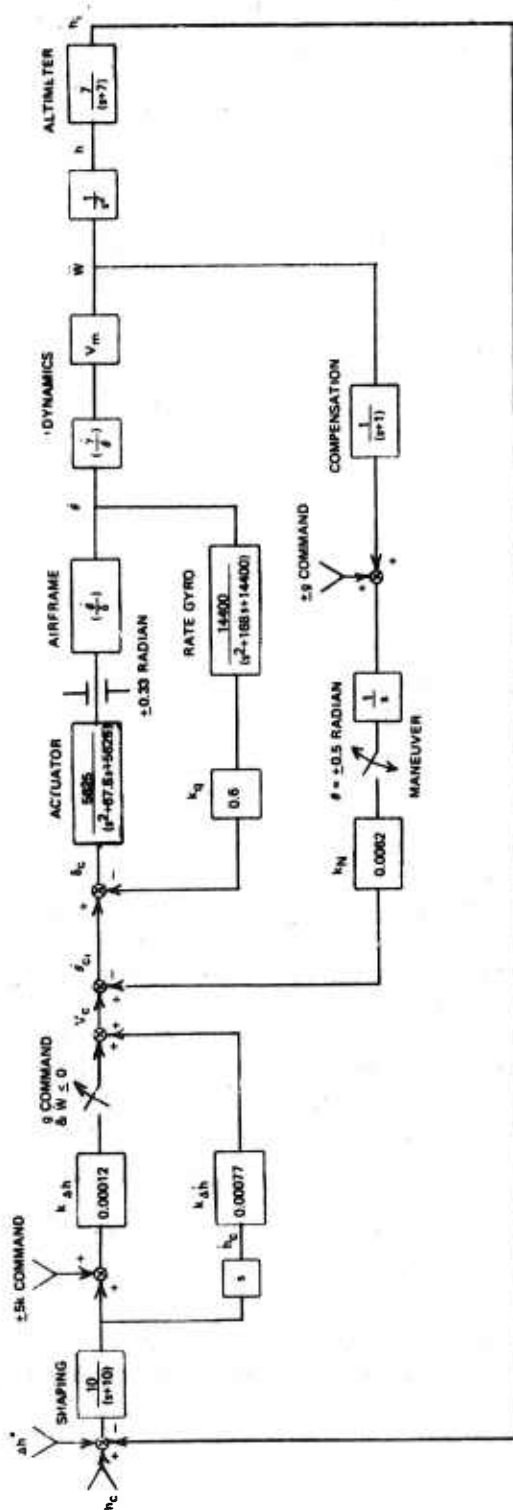
^aInformation obtained from the following contractor document:
 Summary of the Aerodynamic Characteristics of the HAST Target Missile,
 Beech Aircraft Corp. Report, Code Identification No. 70898, January 1973.

The longitudinal rate damping loop transfer function ($\dot{\theta}/\dot{\theta}_c$) was derived from the system block diagram of Figure 1, and the resultant root locus plots are shown in Figures 3 and 4. The $\dot{\theta}/\dot{\theta}_c$ closed loop poles were obtained for the operating gains, and the altitude rate damping loop transfer function (\dot{h}/\dot{h}_c) was derived next. Figures 5 and 6 are the resultant root locus plots obtained. Similarly, the \dot{h}/\dot{h}_c closed loop poles were obtained for the operating gains, and the overall altitude loop or system transfer function (h/h_c) was derived. Figures 7 and 8 are the total system root locus plots, and the stability characteristics determined from all the previous plots are summarized in Table 1.

The g maneuver longitudinal autopilot configuration was analyzed in the same manner. The rate damping loop ($\dot{\theta}/\dot{\theta}_c$) remained the same; while the acceleration loop (\ddot{w}/\dot{v}_c) and altitude rate (\dot{h}/\dot{h}_c) were derived and plotted as previously. Figures 9 to 12 are the resultant \ddot{w}/\dot{v}_c and \dot{h}/\dot{h}_c root locus plots for this autopilot configuration, and the stability characteristics obtained are summarized in Table 1.

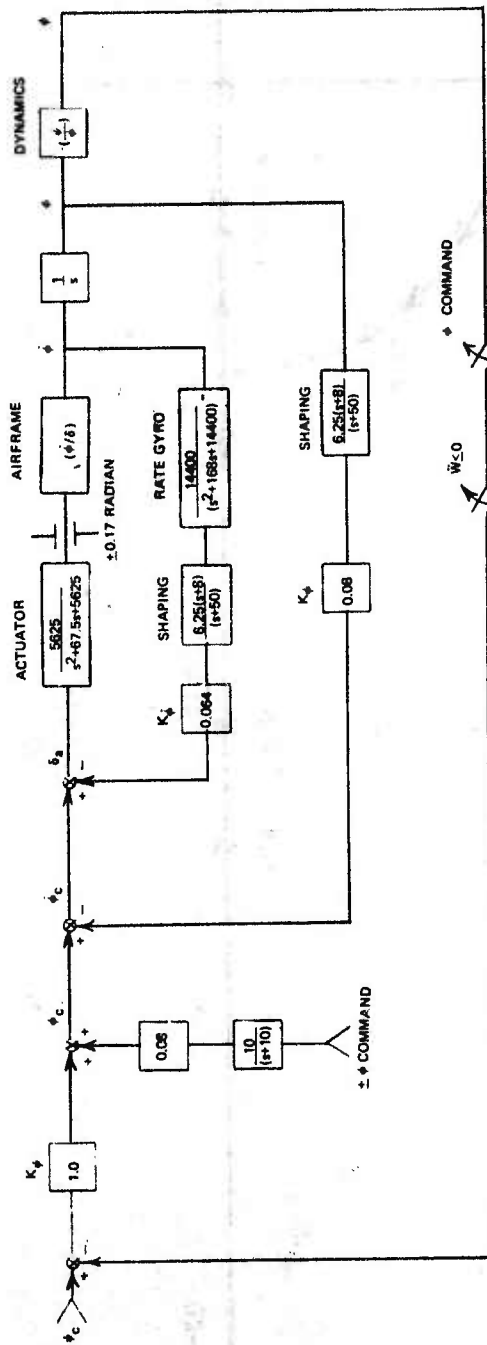
The lateral autopilot, which was analyzed next, consists of a roll rate damping loop, roll attitude loop, and a yaw heading guidance loop. Roll and yaw are coupled in the lateral autopilot because the airframe achieves turning performance through interaction of aerodynamic roll/yaw dynamic coupling. The roll rate damping loop provides stability augmentation to the airframe and increased short period performance capabilities. The roll attitude loop maintains proper roll attitude during flight and is used to achieve the proper yaw maneuvers by control of roll attitude commands. The yaw heading guidance loop provides lateral stable flight throughout the flight profile. The previous loop transfer functions were derived from the system block diagram of Figure 2 and were plotted in the same manner used for the longitudinal analysis. Figure 13 is the roll rate damping loop ($\dot{\phi}/\dot{\phi}_c$) root locus plot; Figure 14 is the roll attitude loop (ϕ/ϕ_c) root locus plot; Figure 15 is the yaw heading (ψ/w_c), or total system root locus plot; and Table 1 gives the resultant stability characteristics.

The results of the stability analysis determined that the system stability characteristics met the flight test requirements of KJ-4.



- (θ/δ) - AIRFRAME TRANSFER FUNCTIONS
 V_m - MISSILE VELOCITY
 $\Delta h^* - (h_c - h_L) \left[\frac{M_c \cdot M_L}{M_c \cdot M_L} \right]^2$
 h_c - CRUISE ALTITUDE (FEET)
 h_L - LAUNCH ALTITUDE (FEET)
- θ - PITCH ATTITUDE (RADIAN)
 (θ/δ) - RATE DAMPING TRANSFER
 (\ddot{w}/δ) - ACCELERATION TRANSFER
 (\dot{w}/δ) - ALTITUDE RATE TRANSFER
 (w/h_c) - ALTITUDE TRANSFER
- h_i - INDICATED ALTITUDE (FEET)
 h - ALTITUDE (FEET)
 \ddot{w} - NORMAL ACCELERATION (FT/SEC²)
 \dot{w} - CALCULATED ALTITUDE RATE (FT/SEC)
 θ - MISSILE PITCH RATE (RAD/SEC)

Figure 1. Longitudinal Autopilot Block Diagram



- (ψ/δ), (ψ/δ) - AIRFRAME TRANSFER FUNCTIONS
- ψ - MISSILE ROLL RATE (RAD/SEC)
- ψ - ROLL ATTITUDE (RADIAN)
- ψ - YAW ATTITUDE (RADIAN)

- (ψ/δ_c) - RATE DAMPING TRANSFER
- (ψ/δ_c) - ROLL ATTITUDE TRANSFER
- (ψ/δ_c) - YAW ATTITUDE TRANSFER

Figure 2. Lateral Autopilot Block Diagram

- X OPEN LOOP POLE
- OPEN LOOP ZERO
- △ CLOSED LOOP K_q DYNAMIC GAIN
- ▲ $K_q = 0.6$ OPERATING GAIN

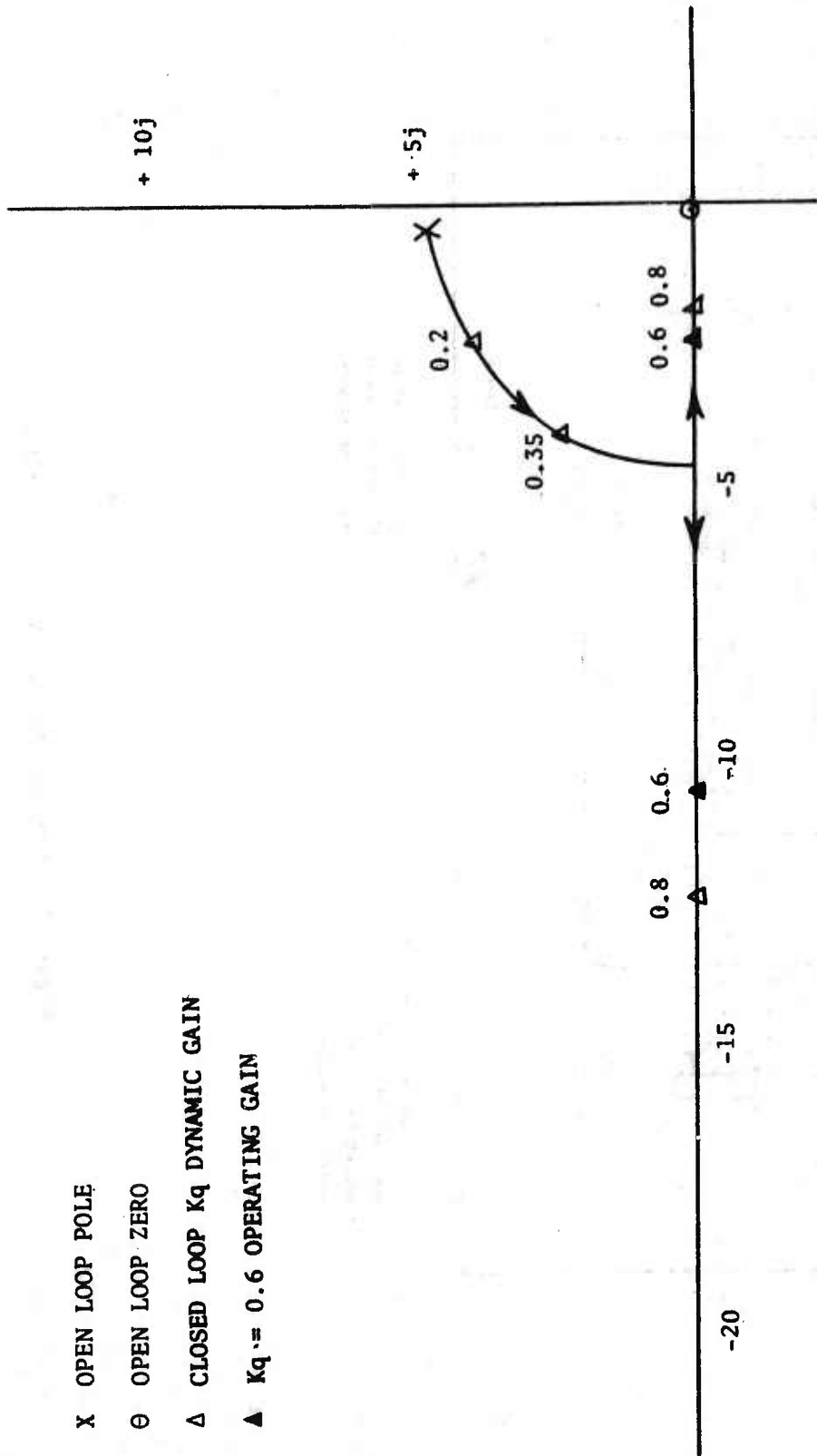


Figure 3. Longitudinal Rate Damping Loop ($\dot{\theta}/\dot{\theta}_c$) - Case 1. Root Locus Plot

- X OPEN LOOP POLE
- OPEN LOOP ZERO
- △ CLOSED LOOP K_q DYNAMIC GAIN
- ▲ $K_q = 0.6$ OPERATING GAIN

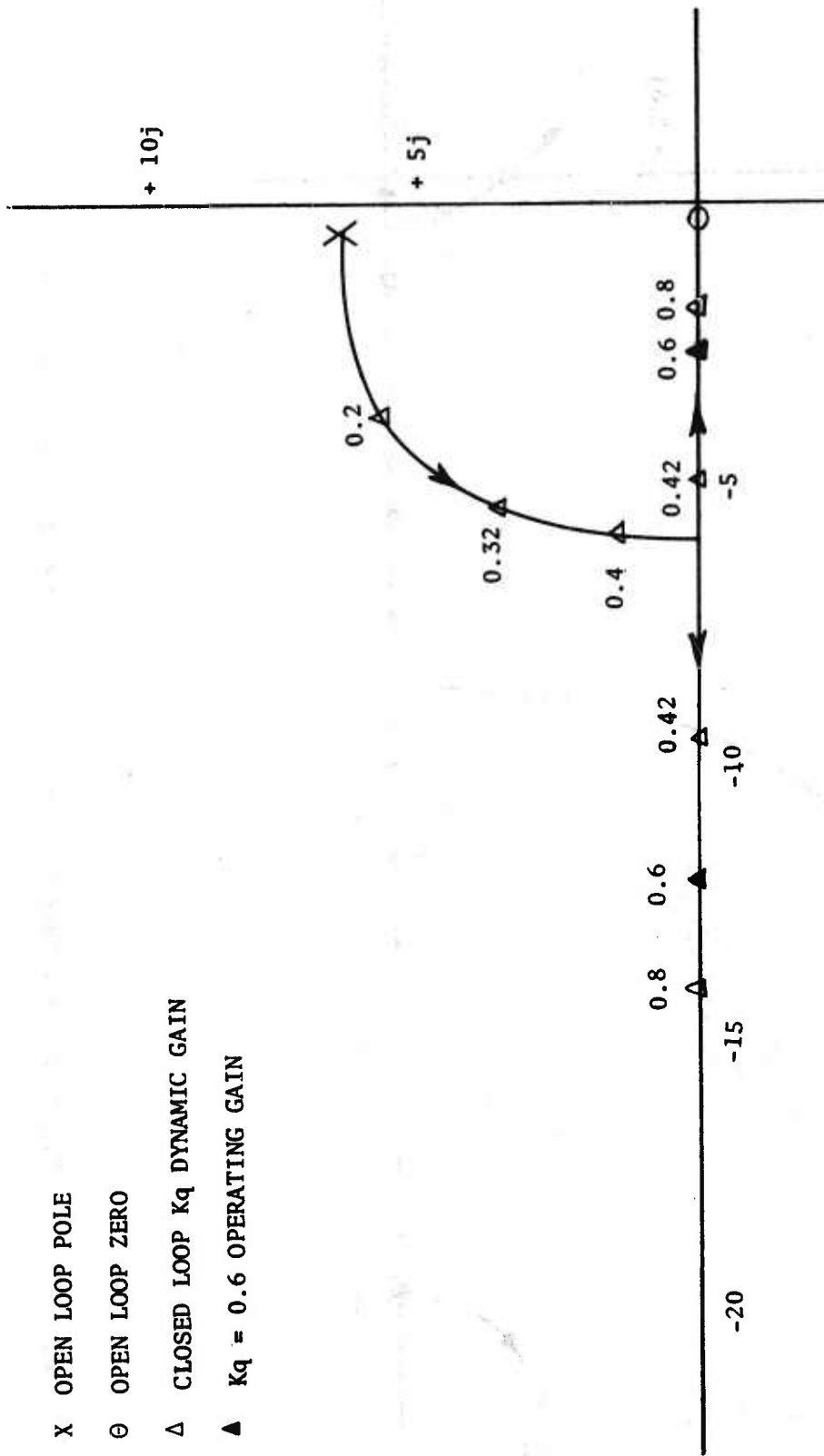


Figure 4. Longitudinal Rate Damping Loop ($\dot{\theta}/\dot{\theta}_c$) - Case 2. Root Locus Plot

- X OPEN LOOP POLE
- ⊖ OPEN LOOP ZERO
- Δ CLOSED LOOP $K_{\Delta h}^*$ DYNAMIC GAIN
- ▲ $K_{\Delta h}^* = 0.00077$ OPERATING GAIN

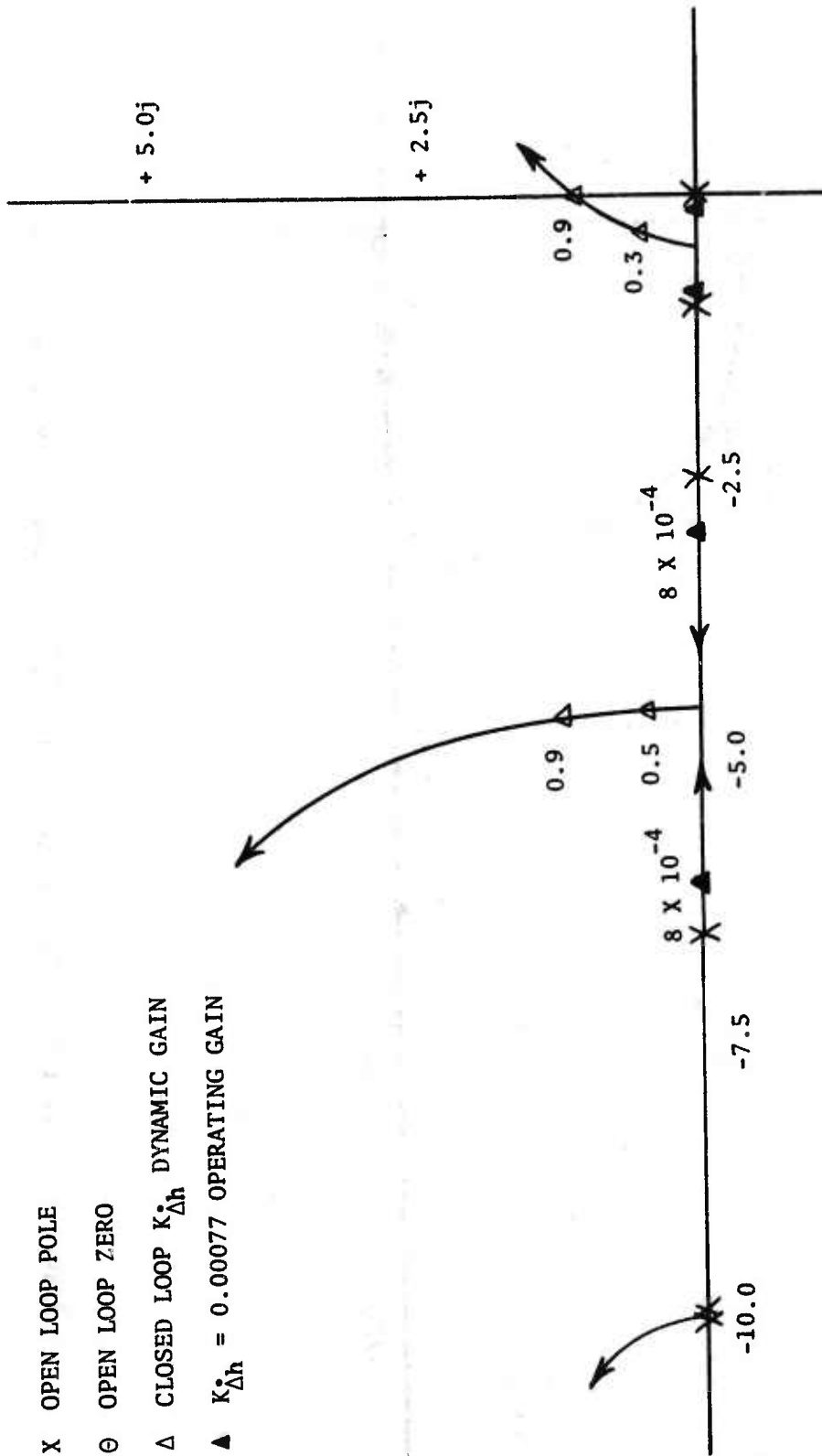
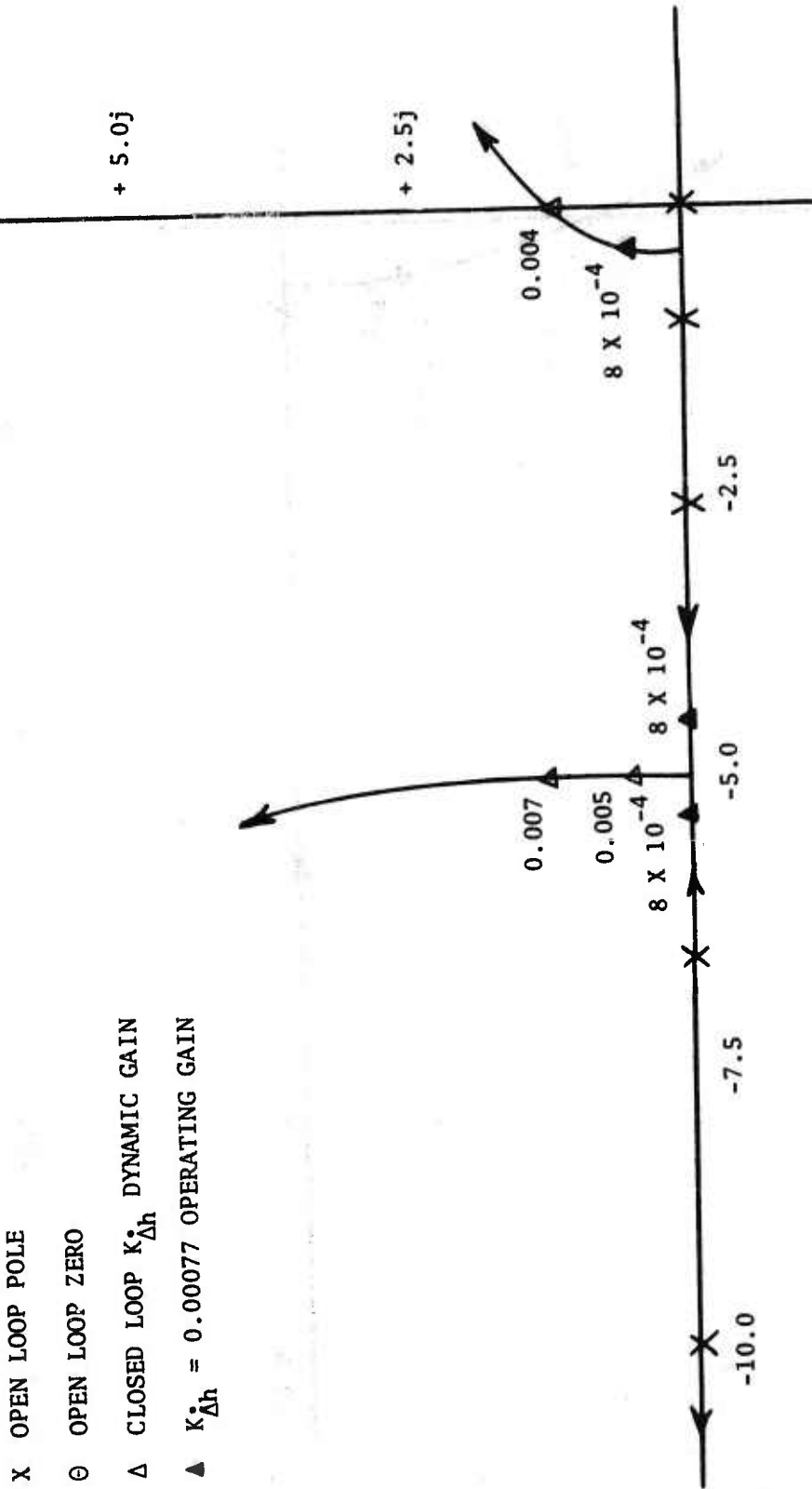


Figure 5. Altitude Rate Loop (\dot{h}/h_c) - Case 1. Root Locus Plot



- X OPEN LOOP POLE
- O OPEN LOOP ZERO
- Δ CLOSED LOOP $K_{\Delta h}$ DYNAMIC GAIN
- ▲ $K_{\Delta h} = 0.00077$ OPERATING GAIN

Figure 6. Altitude Rate Loop (\dot{h}/h_c) - Case 2. Root Locus Plot

- X OPEN LOOP POLE
- ⊖ OPEN LOOP ZERO
- Δ CLOSED LOOP $K_{\Delta h}$ DYNAMIC GAIN
- ▲ $K_{\Delta h} = 0.00012$ OPERATING GAIN

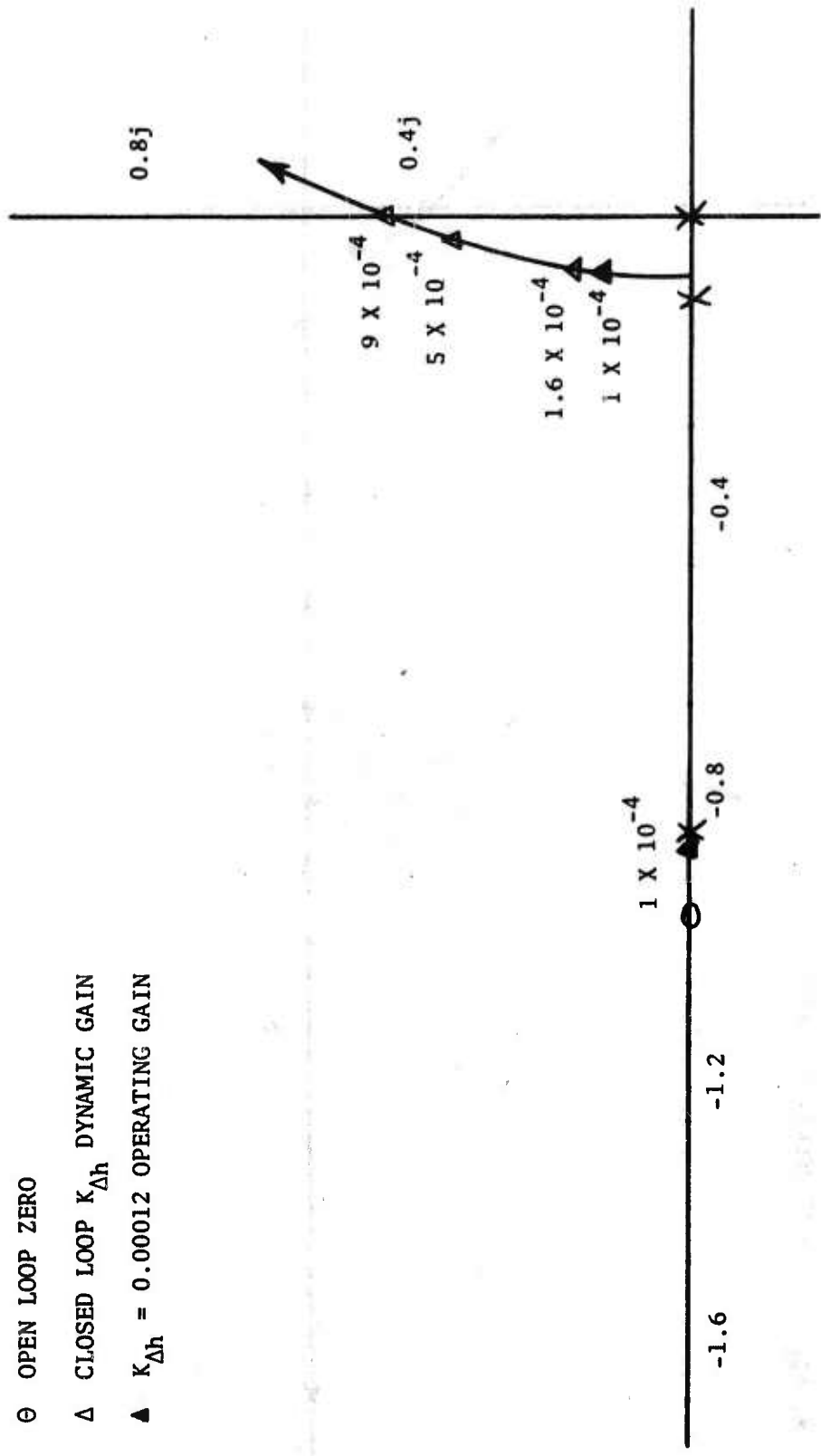


Figure 7. Altitude Loop (h/h_c) - Case 1. Root Locus Plot

- X OPEN LOOP POLE
- ⊖ OPEN LOOP ZERO
- Δ CLOSED LOOP $K_{\Delta h}$ DYNAMIC GAIN
- ▲ $K_{\Delta h} = 0.00012$ OPERATING GAIN

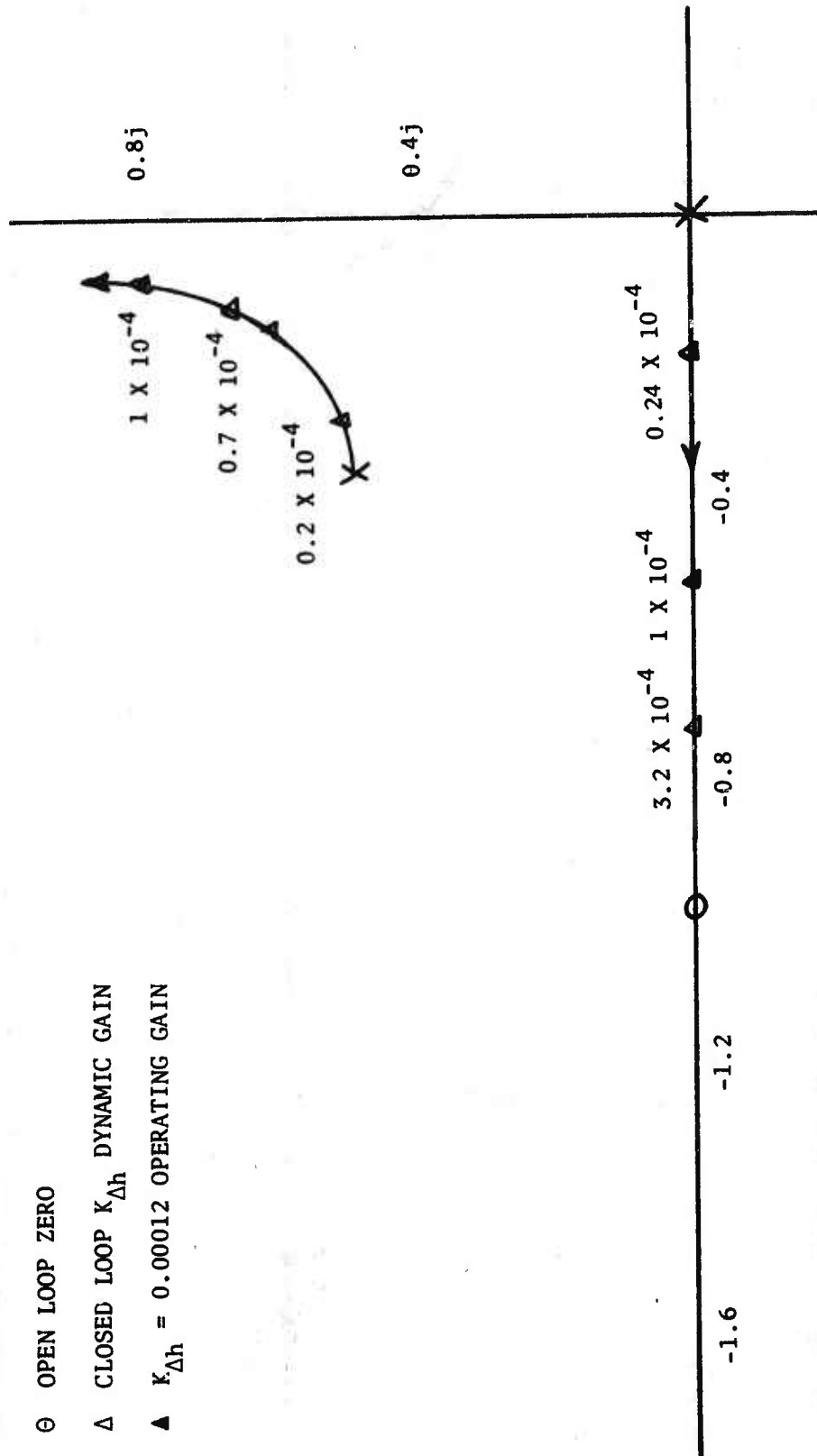


Figure 8. Altitude Loop (h/h_c) - Case 2. Root Locus Plot

- X OPEN LOOP POLE
- OPEN LOOP ZERO
- Δ CLOSED LOOP K_n DYNAMIC GAIN
- ▲ $K_n = 0.0062$ OPERATING GAIN

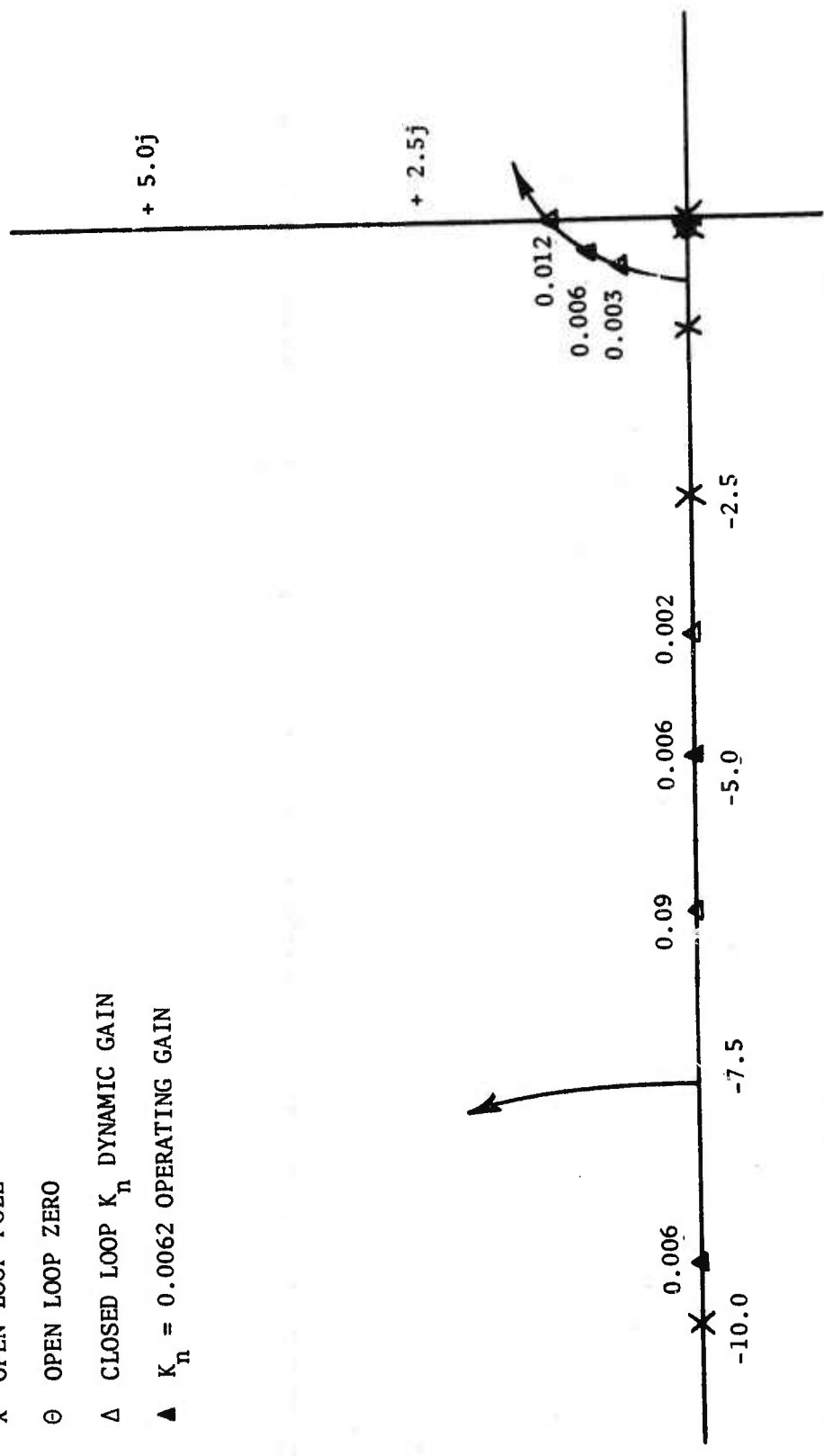


Figure 9. Acceleration Loop (\ddot{W}/V_c) - Case 1. Root Locus Plot

X OPEN LOOP POLE

⊖ OPEN LOOP ZERO

Δ CLOSED LOOP K_n DYNAMIC GAIN

▲ $K_n = 0.0062$ OPERATING GAIN

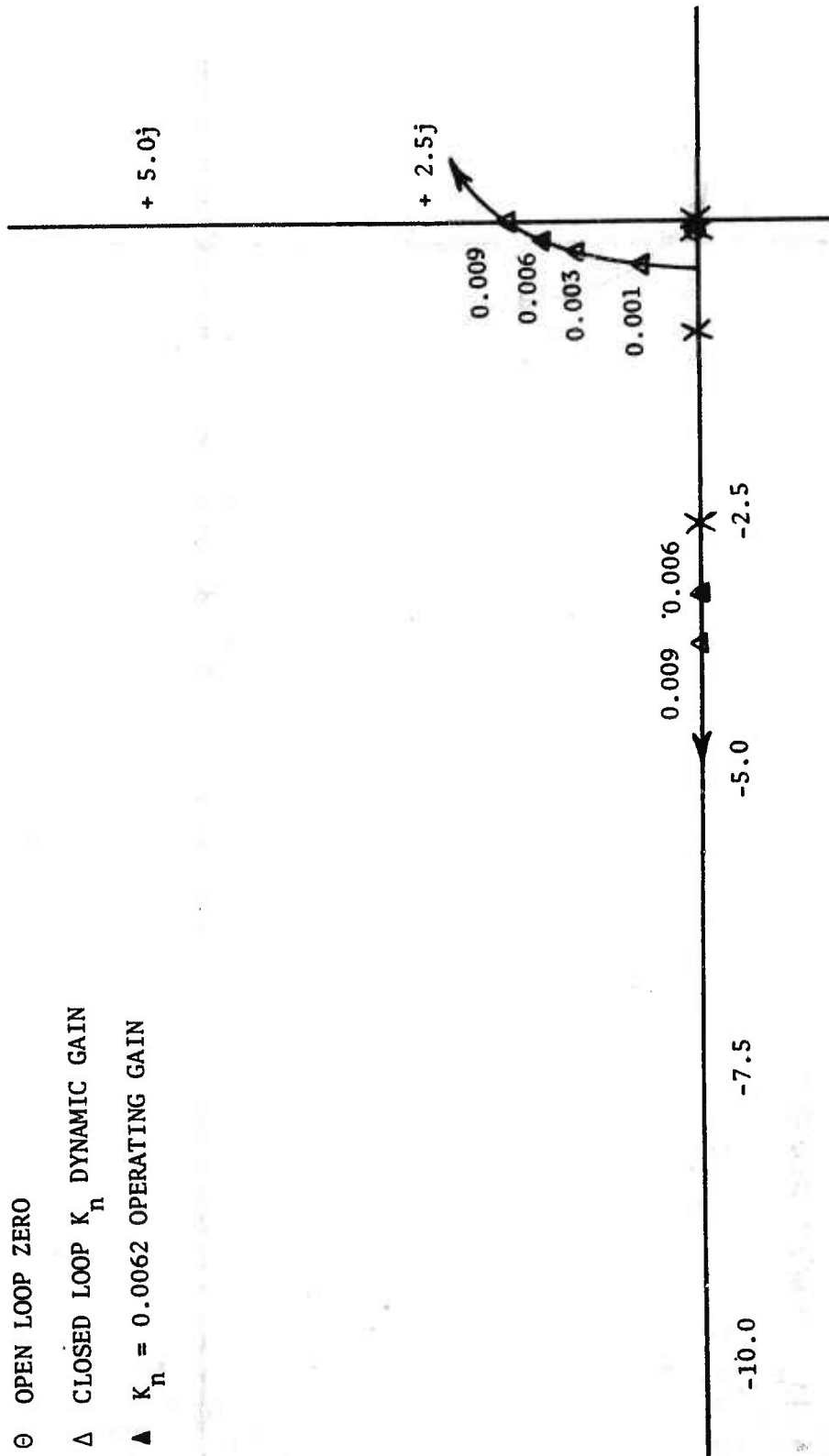


Figure 10. Acceleration Loop (\ddot{W}/V_c) - Case 2. Root Locus Plot

X OPEN LOOP POLE

⊖ OPEN LOOP ZERO

Δ CLOSED LOOP $K_{\Delta h}$ DYNAMIC GAIN

▲ $K_{\Delta h} = 0.00077$ OPERATING GAIN

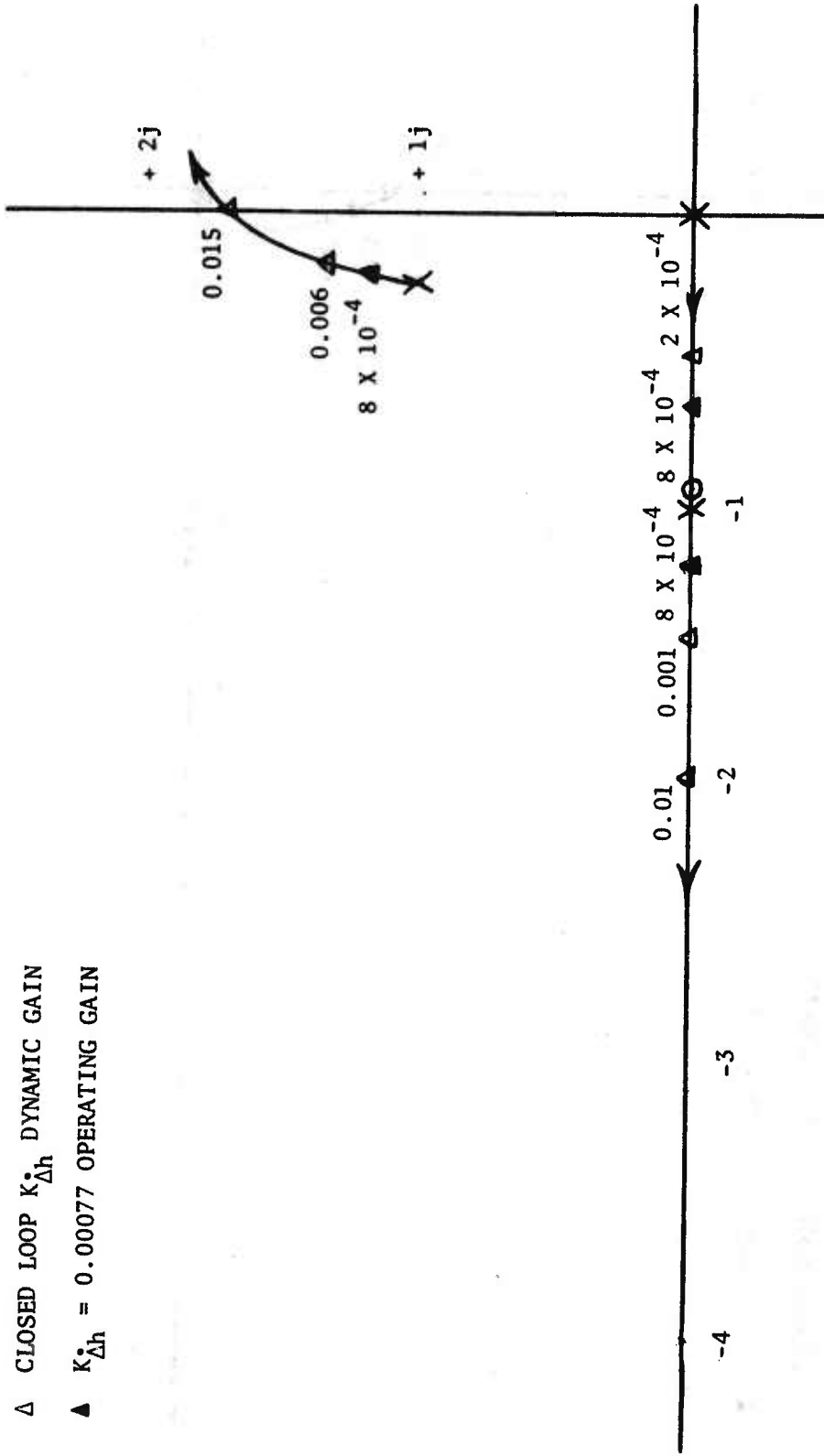


Figure 11. Altitude Rate Loop (\dot{h}/\dot{h}_c), Closed Through (\ddot{w}/V_c) - Case 1, Root Locus Plot

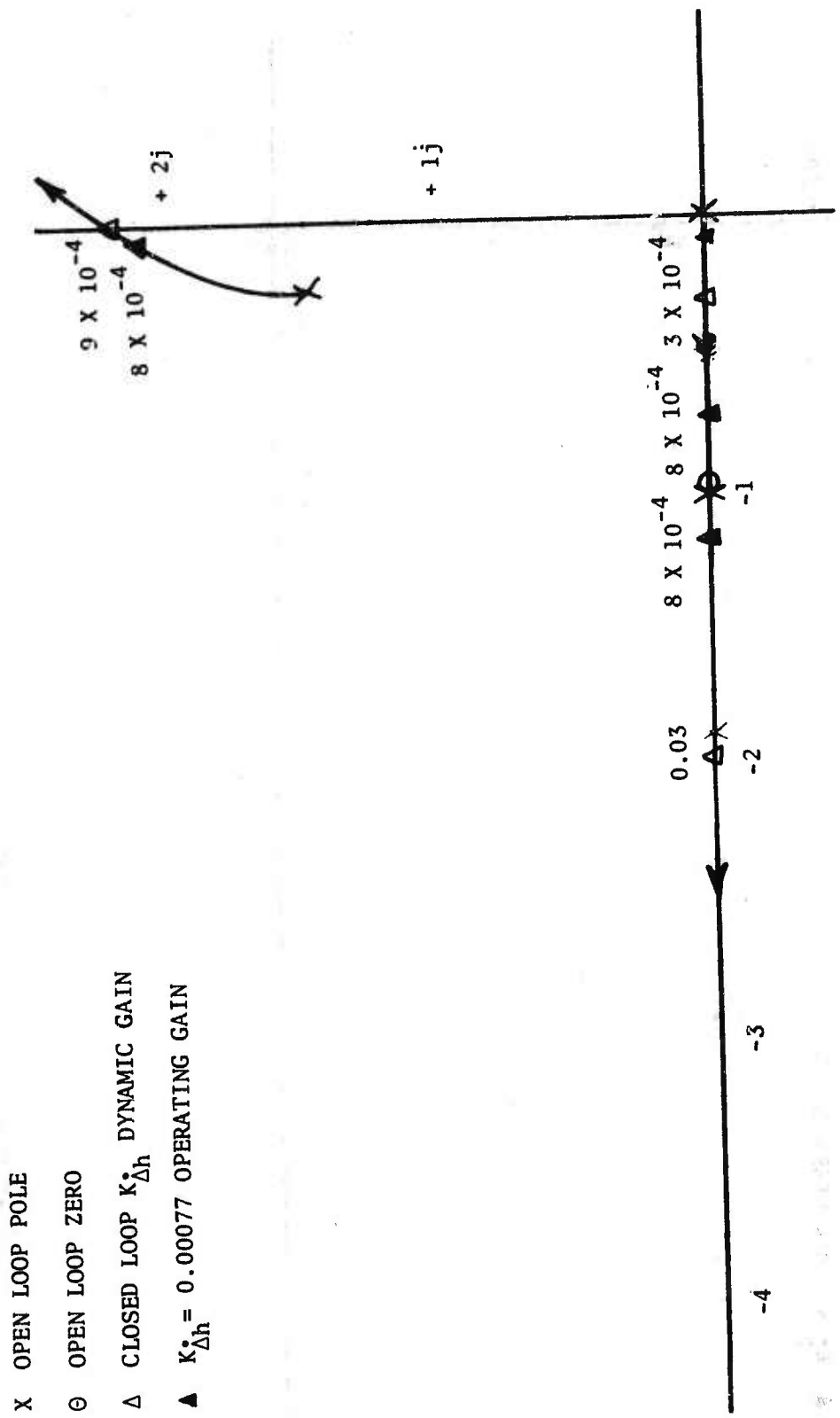


Figure 12. Altitude Rate Loop (\dot{h}/h_c), Closed Through (\ddot{w}/V_c) - Case 2. Root Locus Plot

- X OPEN LOOP POLE
- ⊖ OPEN LOOP ZERO
- Δ CLOSED LOOP K_{ϕ} ; DYNAMIC GAIN
- ▲ $K_{\phi} = 0.054$ OPERATING GAIN

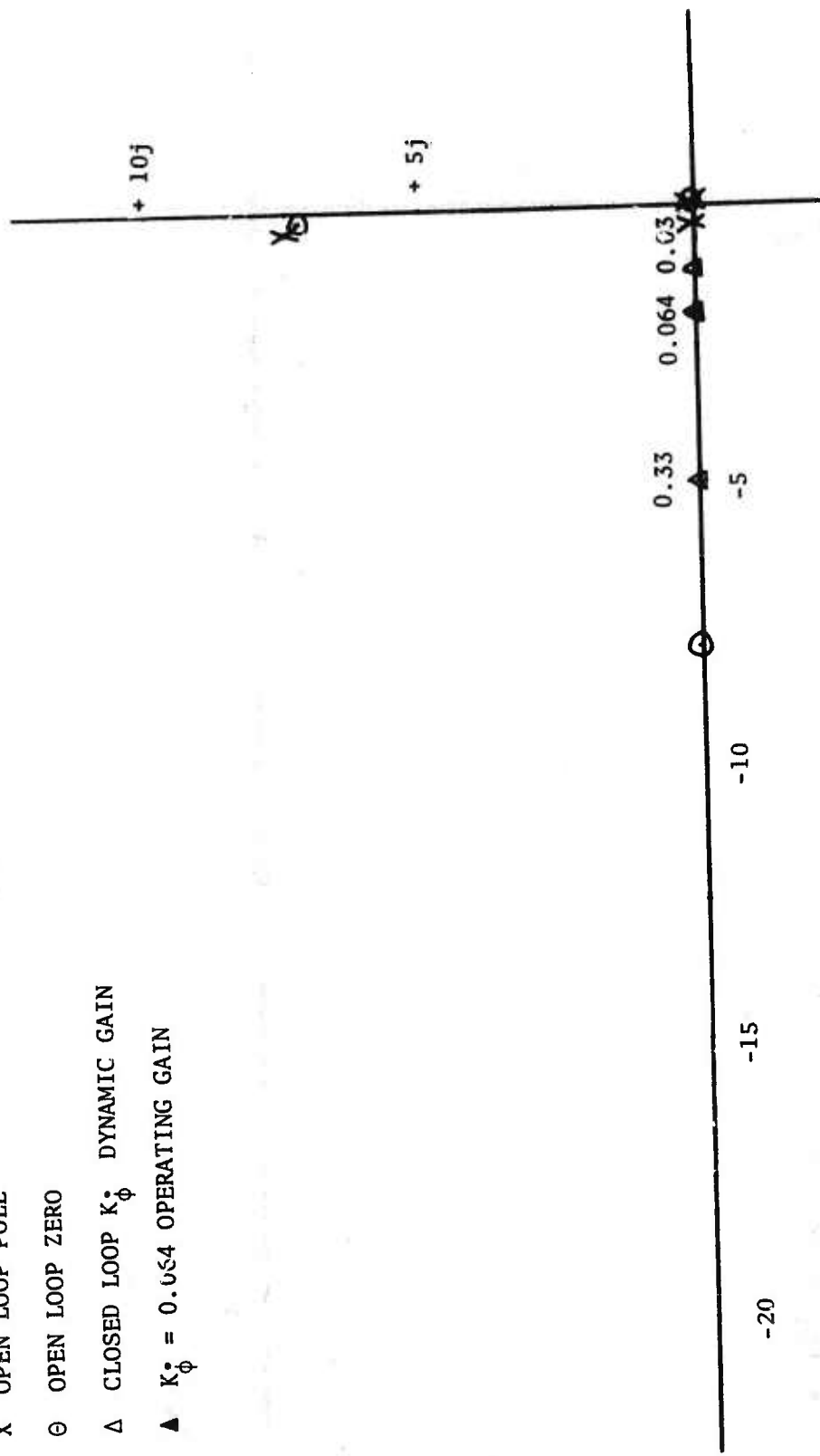


Figure 13. Lateral Rate Damping Loop ($\dot{\phi}/\dot{\phi}_c$) - Case 2. Root Locus Plot

X OPEN LOOP POLE

⊖ OPEN LOOP ZERO

Δ CLOSED LOOP K_ϕ DYNAMIC GAIN

▲ $K_\phi = 0.08$ OPERATING GAIN

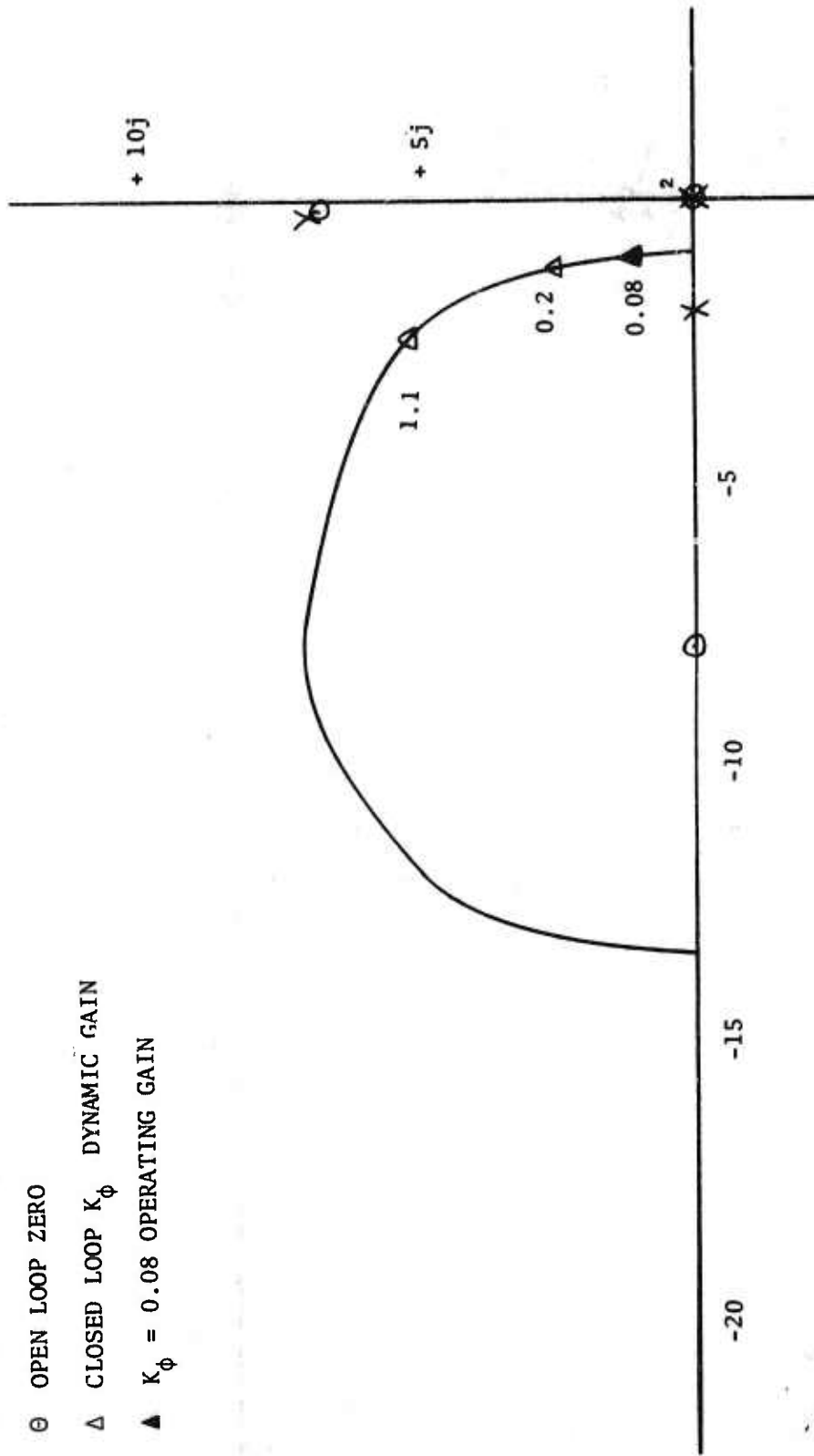


Figure 14. Roll Attitude Loop (ϕ/ϕ_c) - Case 2. Root Locus Plot

- X OPEN LOOP POLE
- ⊖ OPEN LOOP ZERO
- Δ CLOSED LOOP K_{ψ} DYNAMIC GAIN
- ▲ $K_{\psi} = 1.0$ OPERATING GAIN

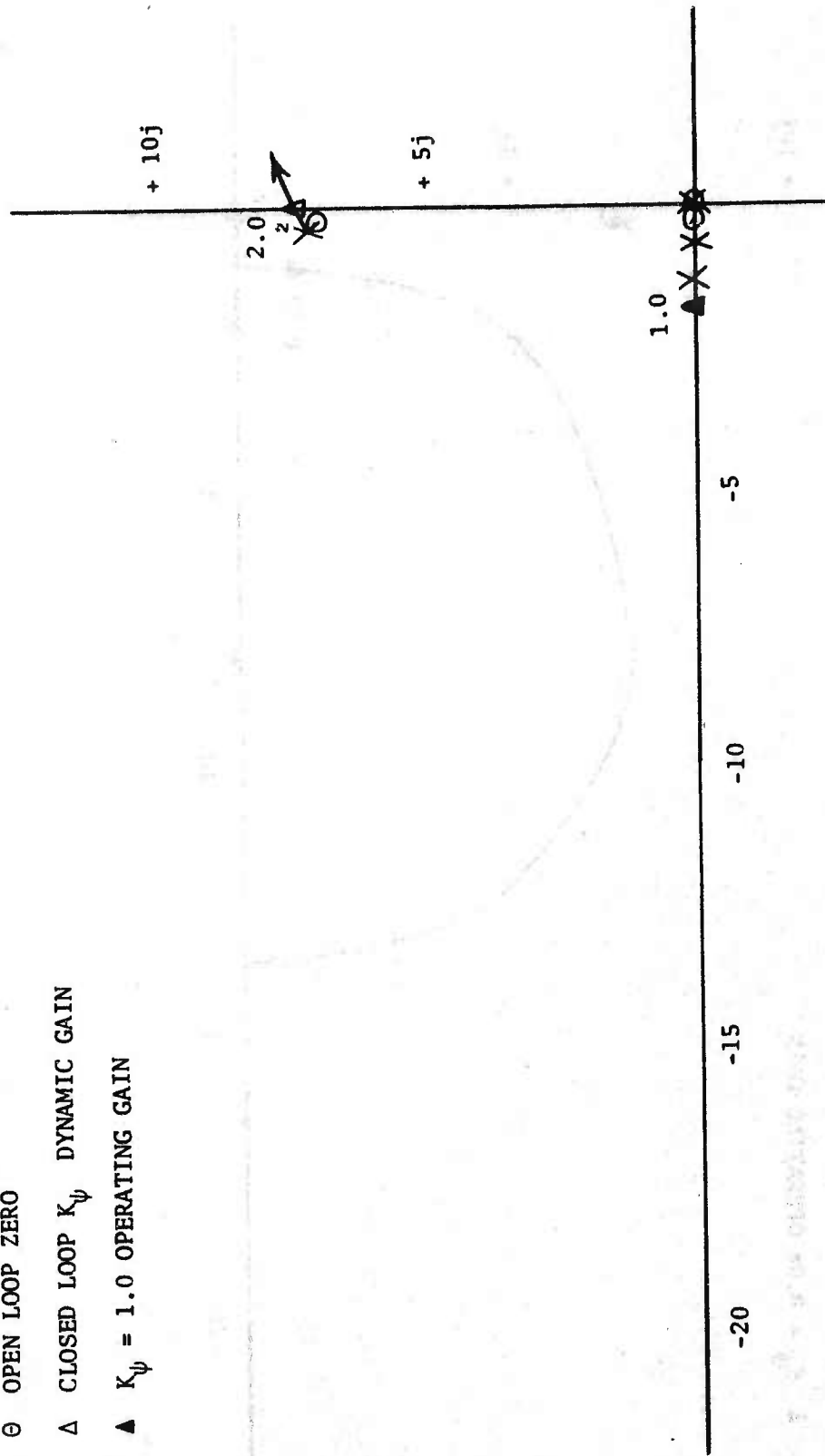


Figure 15. Yaw Attitude Loop (ψ/ψ_c) - Case 2. Root Locus Plot

2. SIMULATION ANALYSIS

A series of simulation analysis studies were performed for evaluation of the previous stability analysis and for determination of the system performance and sensitivities. These studies were performed utilizing digital and hybrid simulation programs. Most of the data were obtained from the six-degrees-of-freedom¹ hybrid simulation developed at Wright-Patterson Air Force Base and maintained by the Air Force Flight Dynamics Laboratory and 4950th Test Wing.

The simulation analysis of the stability cases produced identical results and simultaneously verified the simulation model and the stability analysis results.

The simulation analysis of the system performance and sensitivities investigated the effects of launch transients, autopilot gain variations, thrust misalignment, wind shears and gusts, canard and aileron actuator rates, differentiator noise, and variation of programmed maneuvers. A hybrid simulation analysis summary of the KJ-4 flight test is presented in Table 3. The results obtained were compatible with stability analysis results and determined that the system met the flight test requirements.

¹Further information is presented in the following contractor document: HAST Data Package for Six DOF Hybrid Simulation Employing Hardware Tie-In, Beech Aircraft Corp. Report, Code Identification No. 70898, March 1972.

TABLE 3. PREFLIGHT HYBRID SIMULATION ANALYSIS SUMMARY^{a, b}

1 - 6	Familiarization and autopilot update runs
7	Longitudinal airframe response
8 - 10	Longitudinal pitch rate loop response for K_q variations
11 - 13	Altitude rate loop response for $K_{\Delta h}^{\dot{}}$ variations
14 - 16	Altitude position loop response for $K_{\Delta h}$ variations
17	Lateral airframe response
18 - 20	Roll rate loop response for $K_{\phi}^{\dot{}}$ variations
21 - 23	Roll attitude loop response for K_{ϕ} variations
24	Yaw attitude loop response
27 - 30	Pitch rate launch transient analysis of $\dot{\theta}_{Ic}$
32 - 33	Pitch rate launch transient analysis of K_q and $\dot{\theta}_{Ic}$
34 - 37	Roll rate launch transient analysis of $\dot{\theta}_{Ic}$
38 - 39	Roll rate launch transient analysis of $K_{\phi}^{\dot{}}$ and $\dot{\phi}_{Ic}$
40 - 42	Pitch and roll rate transient analysis of K_q and $K_{\phi}^{\dot{}}$
43 - 45	Thrust misalignment in pitch plane
46 - 48	Thrust misalignment in yaw plane
51 - 52	Vertical wind shear analysis
53 - 54	Lateral wind gust analysis
54a	Combination of vertical and lateral winds
55 - 56	Canard and aileron actuator rate analysis
57	Δh differentiator noise
59 - 61	Varying KJ-4 runs with combined maneuvers

^a $K_q, K_{\Delta h}^{\dot{}}, K_{\Delta h}, K_{\phi}^{\dot{}}, K_{\phi}$ are appropriate autopilot gains

^b $\dot{\theta}_{Ic}, \dot{\phi}_{Ic}$ denotes initial conditions

SECTION III

FLIGHT TEST RESULTS

The real time guidance and control parameters for the KJ-4 flight test are shown in Figures 16 to 25. The required launch conditions were met, and the flight test was initiated. From 5 minutes prior to launch until 39 seconds after launch, telemetry data indicated proper system operation. All voltages, currents, event sequencing, engine ignition, boost thrust, and commanded events appeared to operate normally. Dynamically, the missile experienced a normal launch with the introduction of nominal launch transients. A pitch oscillation was noted at launch, but upon activation of the longitudinal autopilot, this was quickly damped out. The missile lost altitude due to the effects of gravity and launcher kick, and the control system responded by commanding increasingly positive canard deflections. As the missile approached cruise altitude, the canard position went to a full negative attitude and then reversed to a full positive attitude. It became evident at this point that the longitudinal autopilot was not maintaining stable flight.

In the lateral plane, the missile achieved a flight trim roll attitude to counteract the effects of fin misalignment and wind gusts. A steady-state dynamic condition was achieved; but at approximately 10 seconds after launch, large roll rates were experienced by the system. These large roll rates occurred concurrently with the excessive pitch excursions as the result of dynamic coupling. At 12 seconds after launch, intermittent aileron operation was observed via the telemetry data. The system was unstable at this time, and intermittent aileron operation appeared to be a secondary effect.

The complete flight test objectives of the KJ-4 flight test mission were not met, but critical data were obtained for evaluation.

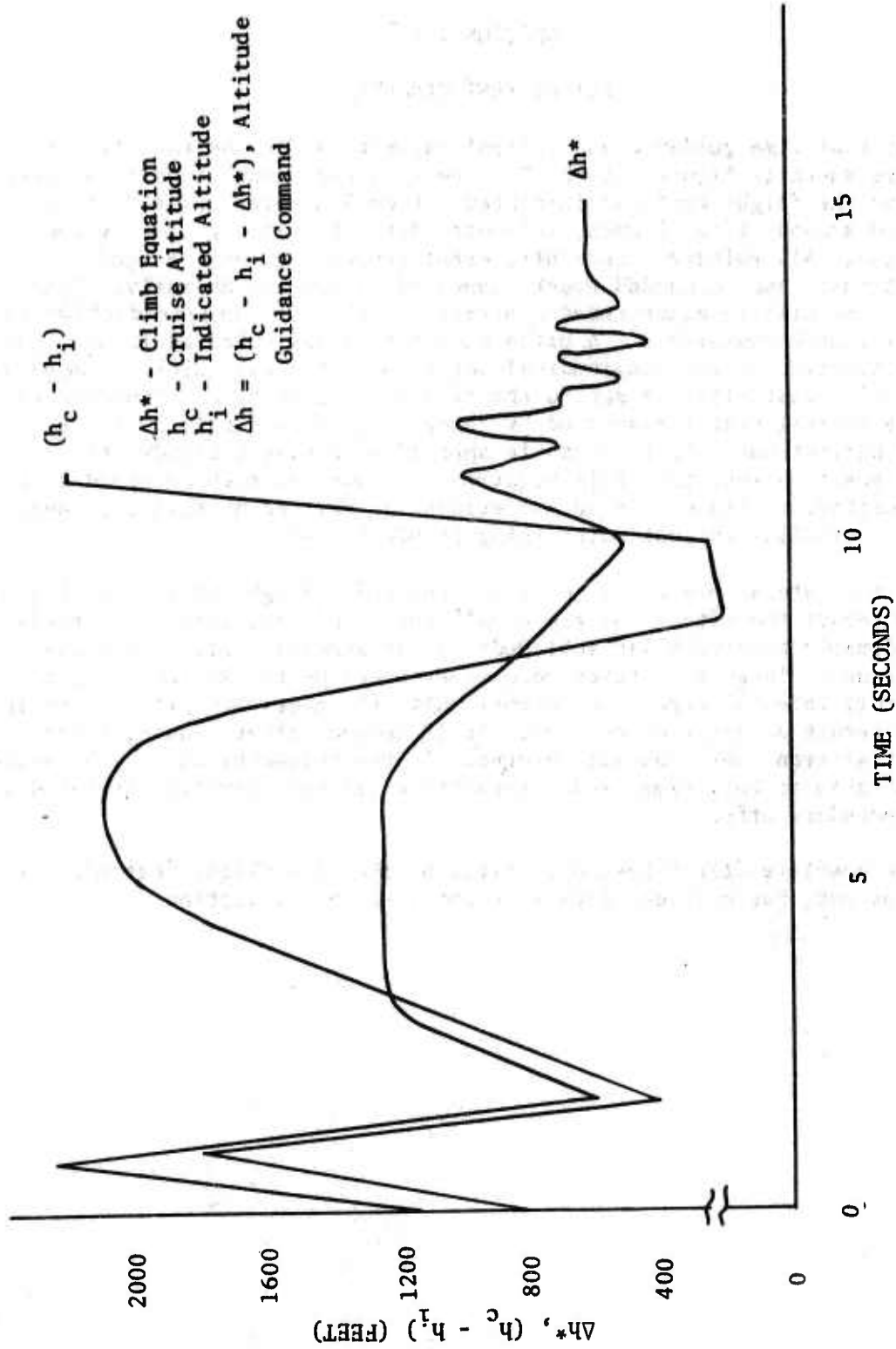


Figure 16. Δh^* , $(h_c - h_i)$ vs Time - Flight Test Results

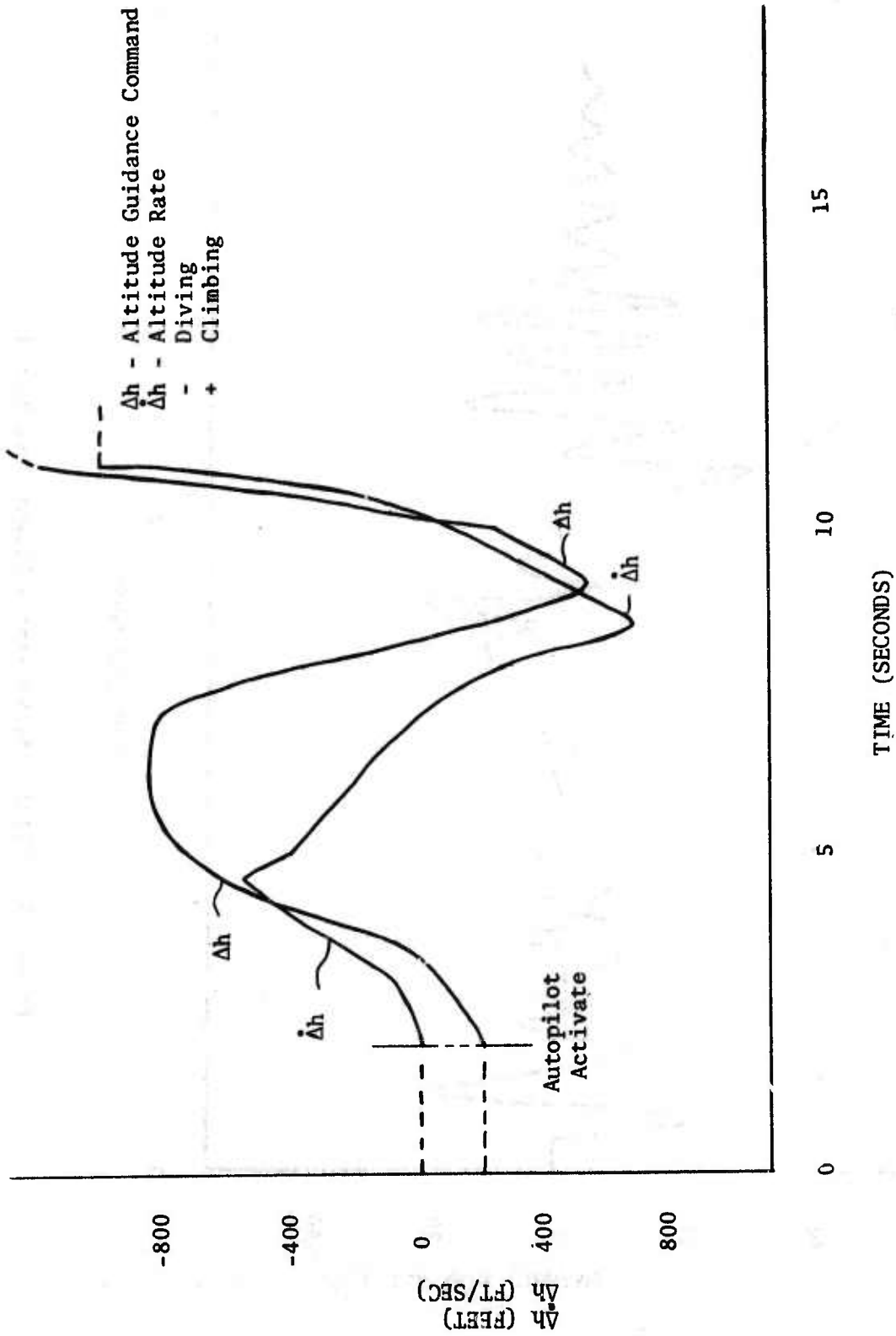


Figure 17. Altitude, Altitude Rate vs Time - Flight Test Results

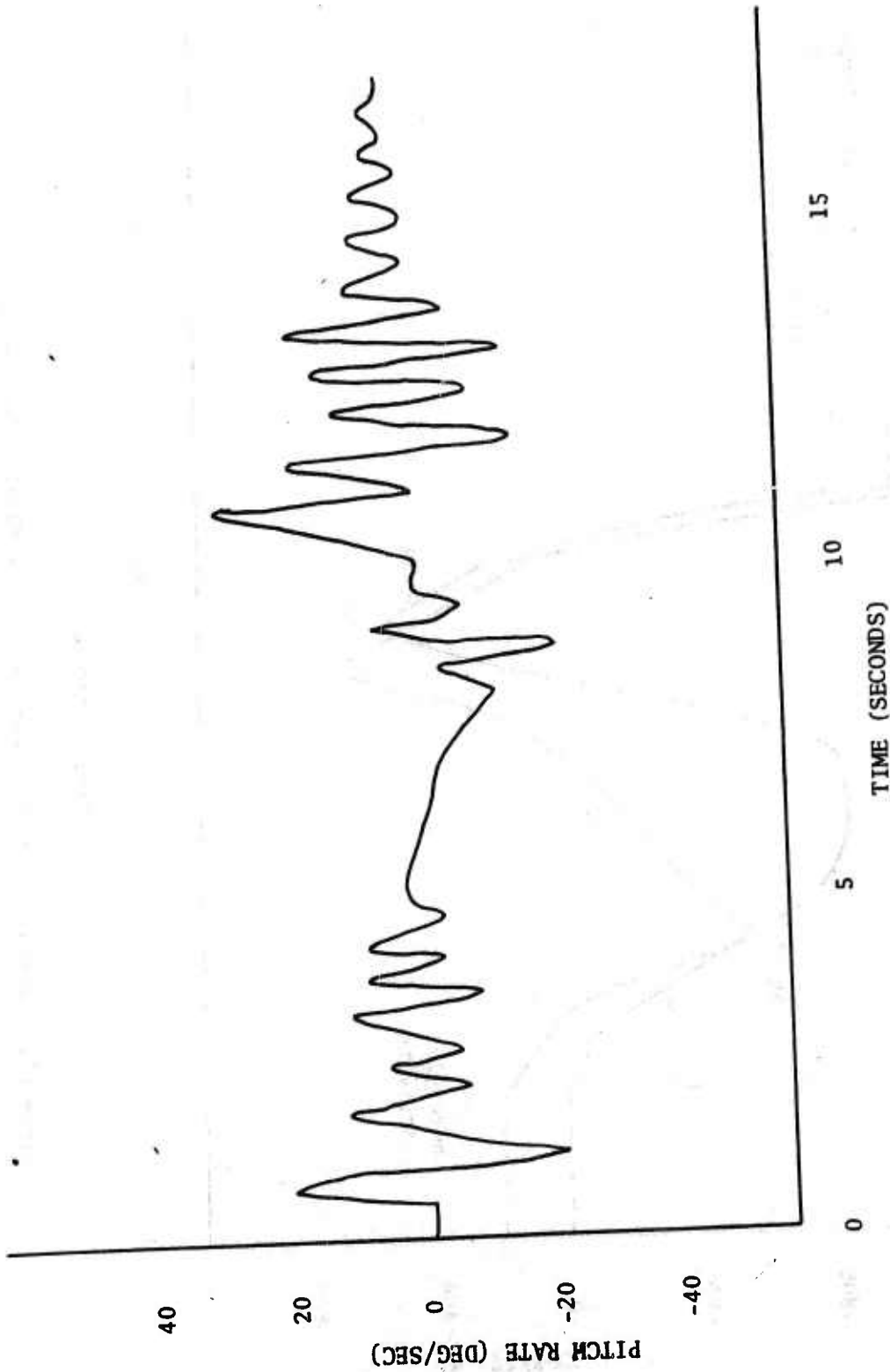


Figure 18. Pitch Rate vs Time - Flight Test Results

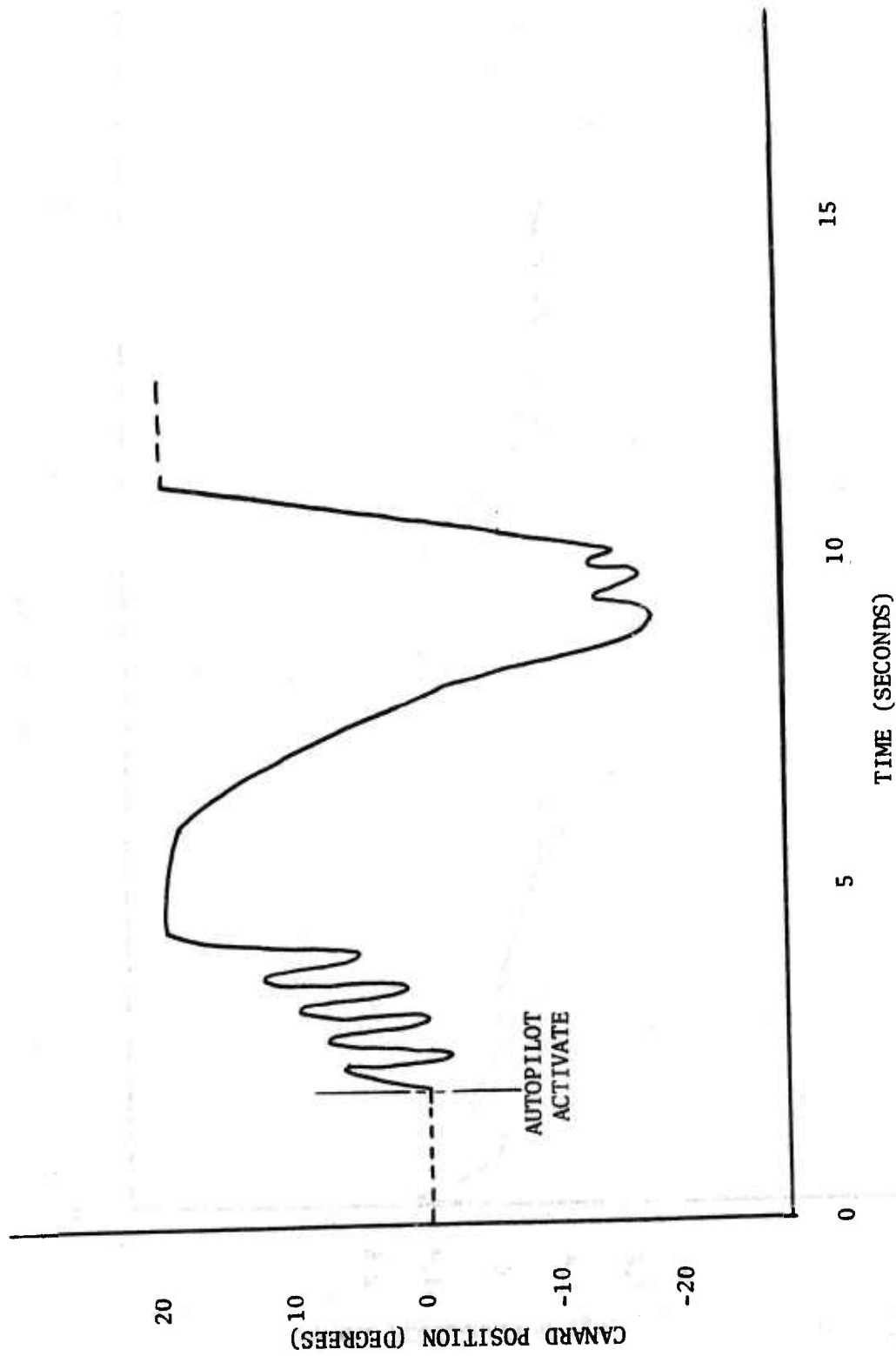


Figure 19. Canard Position vs Time - Flight Test Results

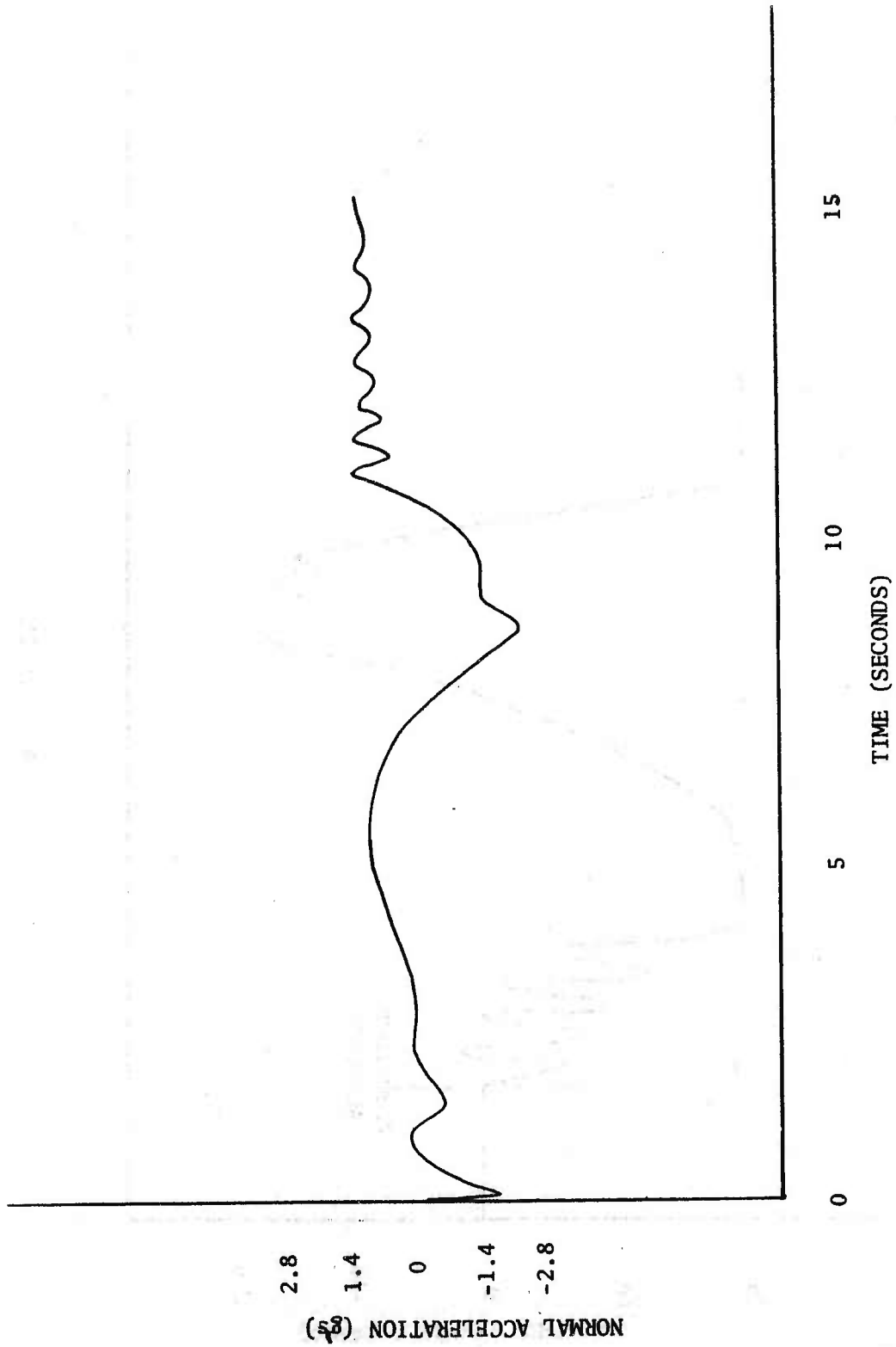


Figure 20. Normal Acceleration vs Time - Flight Test Results

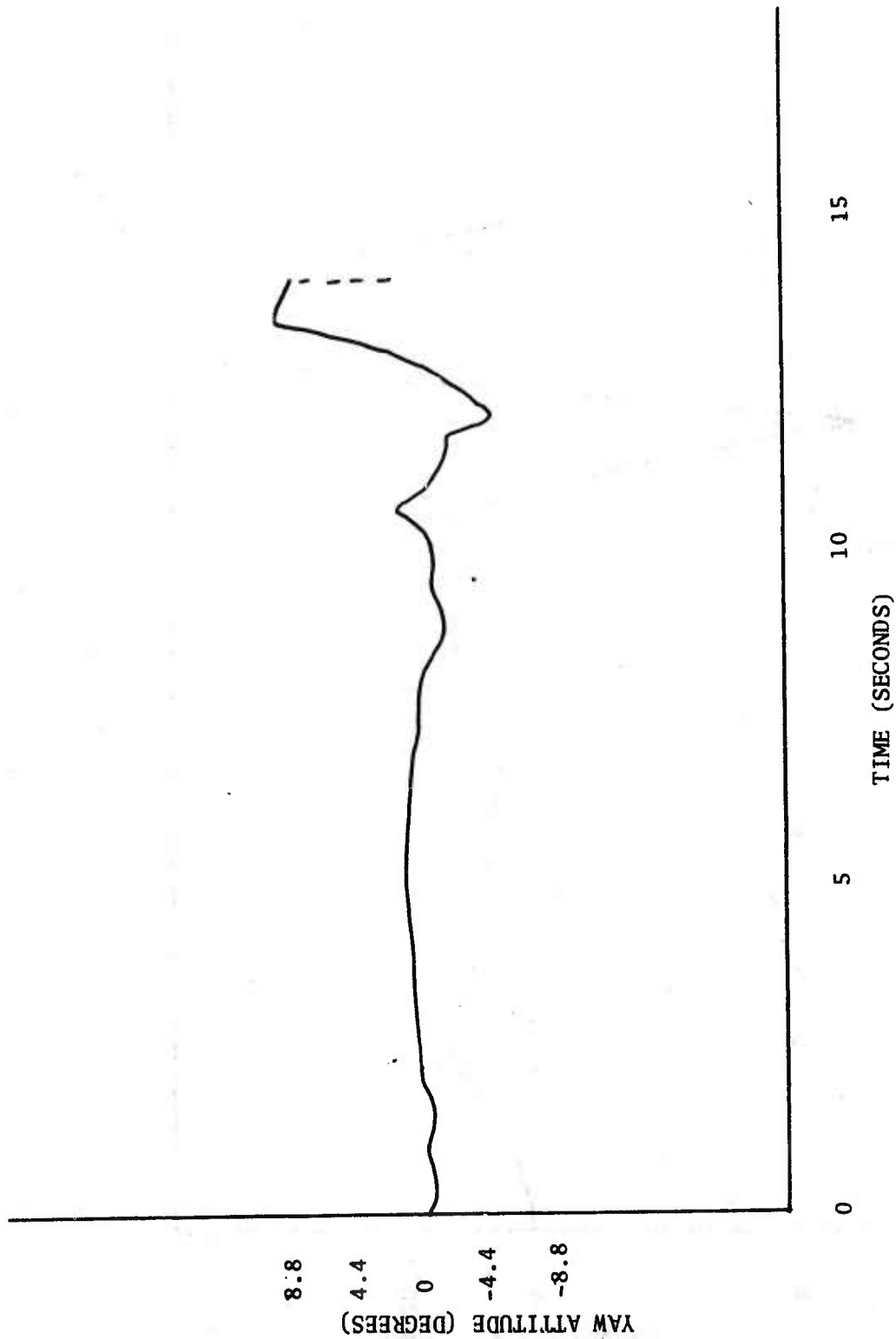


Figure 21. Yaw Attitude vs Time - Flight Test Results

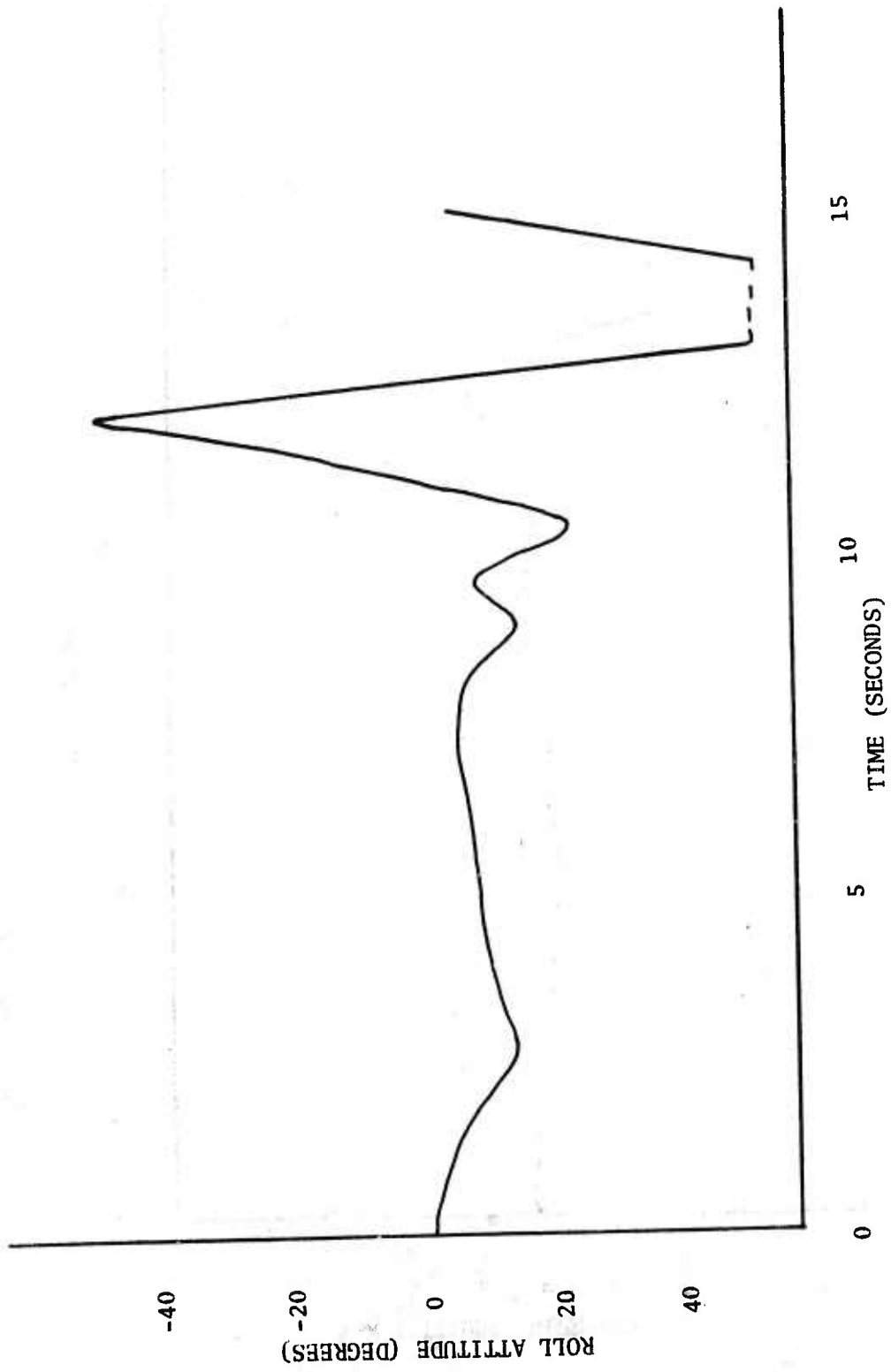


Figure 22. Roll Attitude vs Time - Flight Test Results

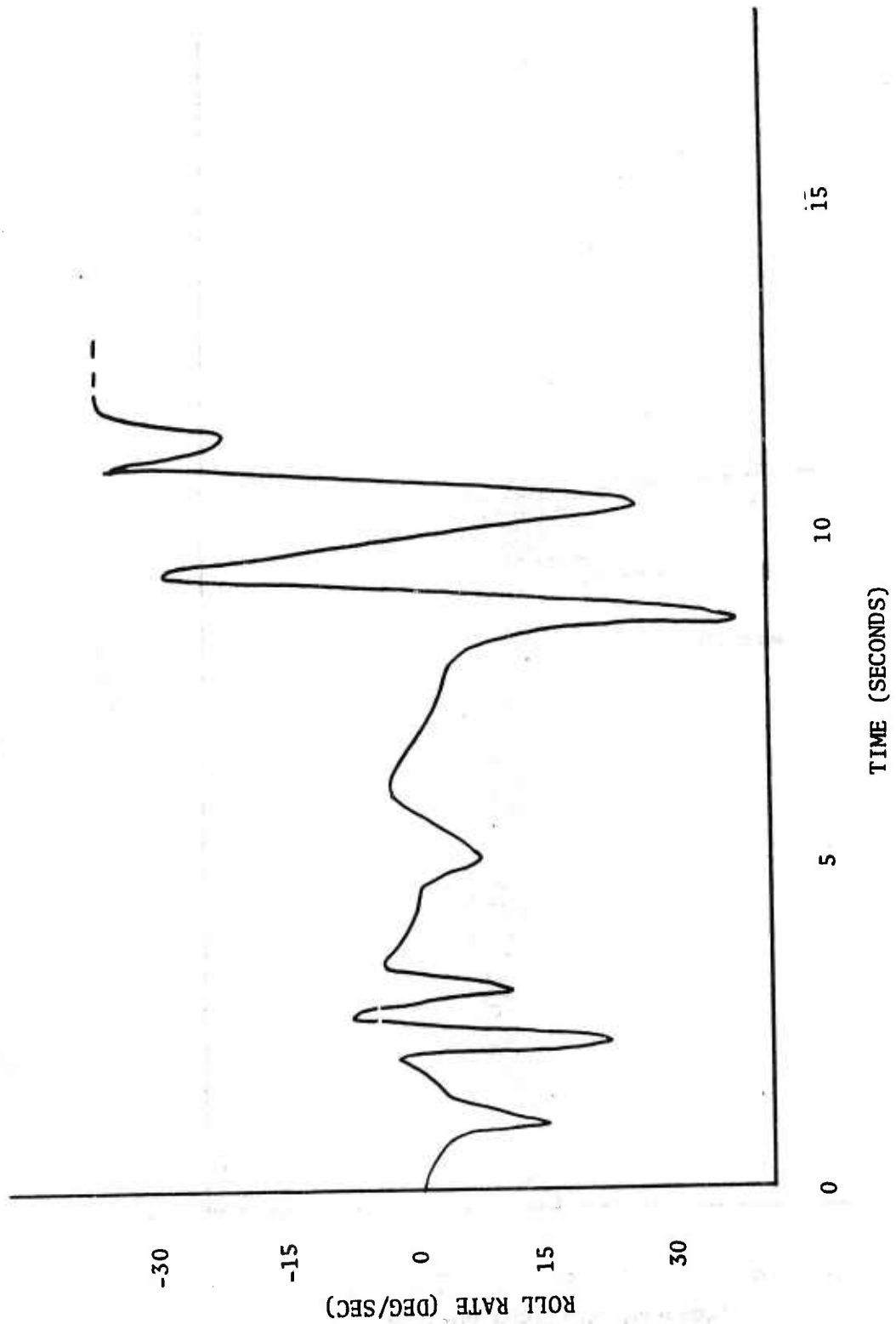


Figure 23. Roll Rate vs Time - Flight Test Results

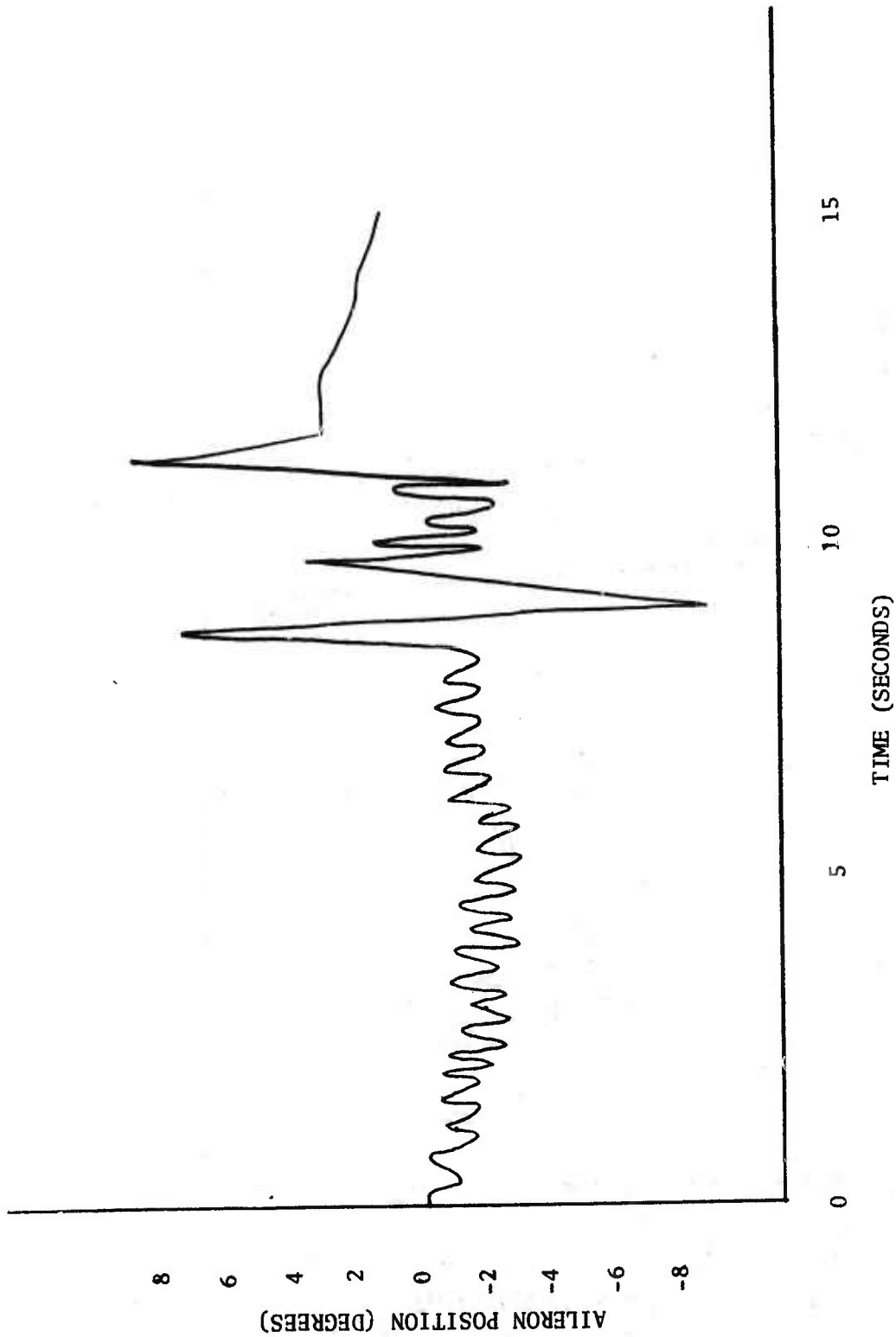


Figure 24. Aileron Position vs Time - Flight Test Results

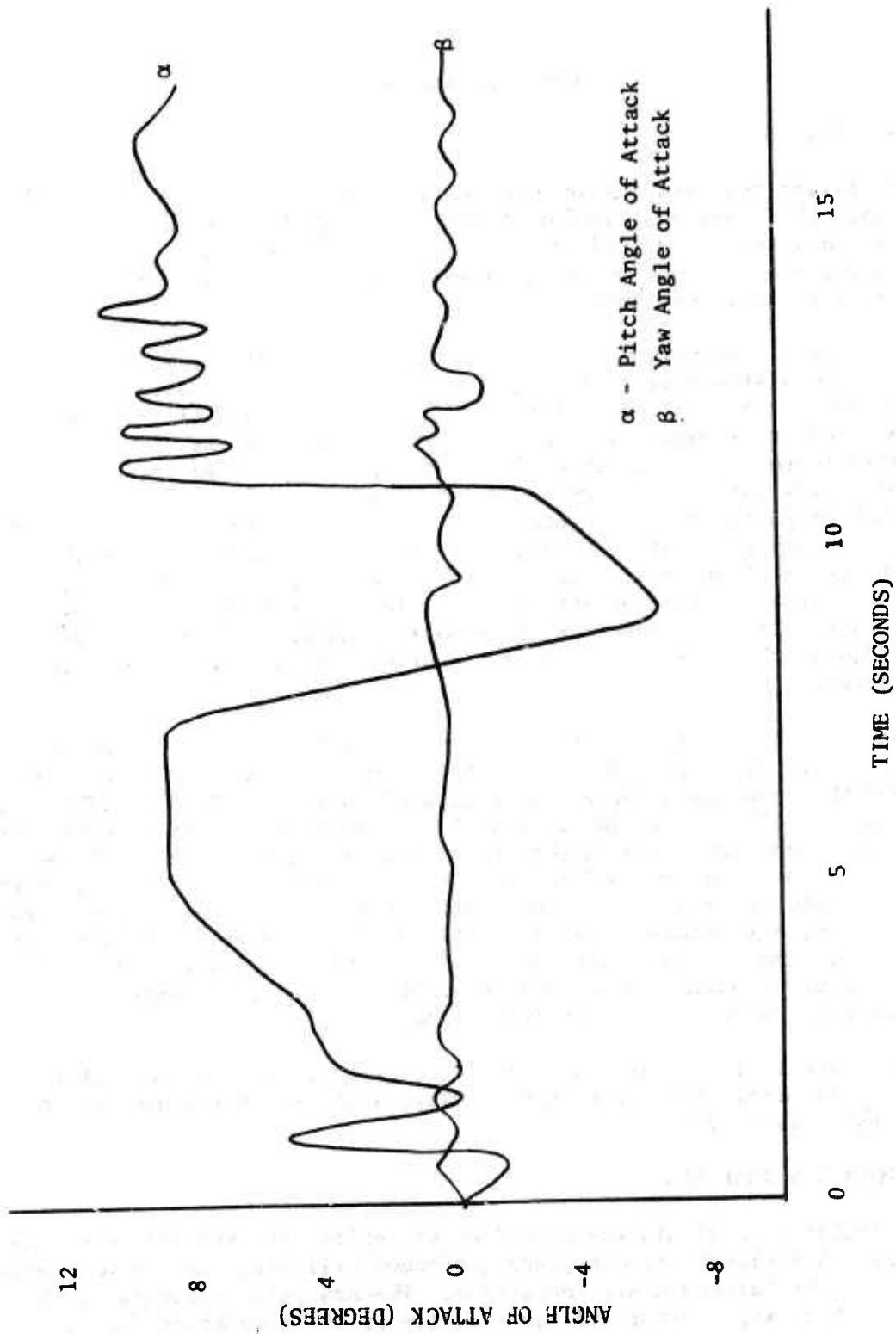


Figure 25. Angle of Attack vs Time - Flight Test Results

SECTION IV

POSTFLIGHT ANALYSIS

1. DATA ANALYSIS

The flight test results were evaluated by utilizing a cause and effect approach. The individual autopilot guidance signals were identified and verified, and the calculated control command was compared to the actual control position. Since the longitudinal autopilot characteristics were most suspect, they were analyzed first.

The initial evaluation of the longitudinal autopilot resulted in verifying proper system operation. Figure 26 shows that the control command matched the flight test control position. Further evaluation of the guidance sensors showed that indicated altitude did not match radar altitude data (Figure 27). Reevaluation of the data disclosed that the indicated attitude transient response characteristics were identical to the angle-of-attack characteristics (Figure 28). This was attributed to the pitot static tube being sensitive to angle-of-attack variations and resulted in the generation of destabilizing altitude guidance signals equivalent to 100 feet per degree of angle of attack. All other operations of the longitudinal autopilot were functioning normally, and this altitude error was identified as the cause of the system instability; a simulation analysis was started.

The lateral autopilot operated properly for the first 8 seconds after flight. During this period, the control command was normal, except for a larger than nominal aileron oscillation (Figure 29). This is attributed to hardware mechanization and component tolerances of the (0.125S+1) lateral shaping compensation. The flightpath is unaffected since the airframe filters this oscillation, but the main concern here is with the resultant actuator wear. From 8 to 11 seconds after launch, the large pitch transients dynamically coupled into the lateral plane and produced large lateral transients. The system became uncontrollable at that point. An intermittent aileron actuator operation was also observed but had negligible effect because the system was already in an unstable condition.

As a result of the data analysis, further studies were undertaken to evaluate the pitot static tube sensitivity, which was the source of the pitch instability problem.

2. SIMULATION ANALYSIS

A simulation analysis was conducted to verify the data analysis conclusions. A series of studies were performed utilizing the hybrid simulation at Wright-Patterson Air Force Base. The analysis investigated the flight test altitude error and the accuracy of the simulation model.

The altitude error was introduced into the simulation model with the following equation:

$$h_m = h - K_\alpha \alpha \quad (1)$$

Where h_m is the measured altitude, h is the real altitude, K_α is the altitude error constant, and α is the angle of attack. The analysis showed that for $K_\alpha = 100$ feet/degree, the simulation data were identical to the flight test results. Figure 30 shows a comparison between simulation and flight test data of the canard position parameter. The remaining longitudinal parameters were compared with the flight test data and provided identical results.

Additionally, a simulation analysis was undertaken to verify the simulation model accuracy when compared with dynamic flight test data. This was accomplished by performing an open loop simulation of the model, using the canard and aileron actuator positions from the flight test data as forcing functions. The resultant simulation data were comparable to the flight test results and provided dynamic verification between the simulation model and the actual system operation.

The simulation analysis concluded that a $K_\alpha = 100$ feet/degree was the cause of the KJ-4 flight test instability. In addition, the accuracy of the simulation model was determined to match the system operational characteristics.

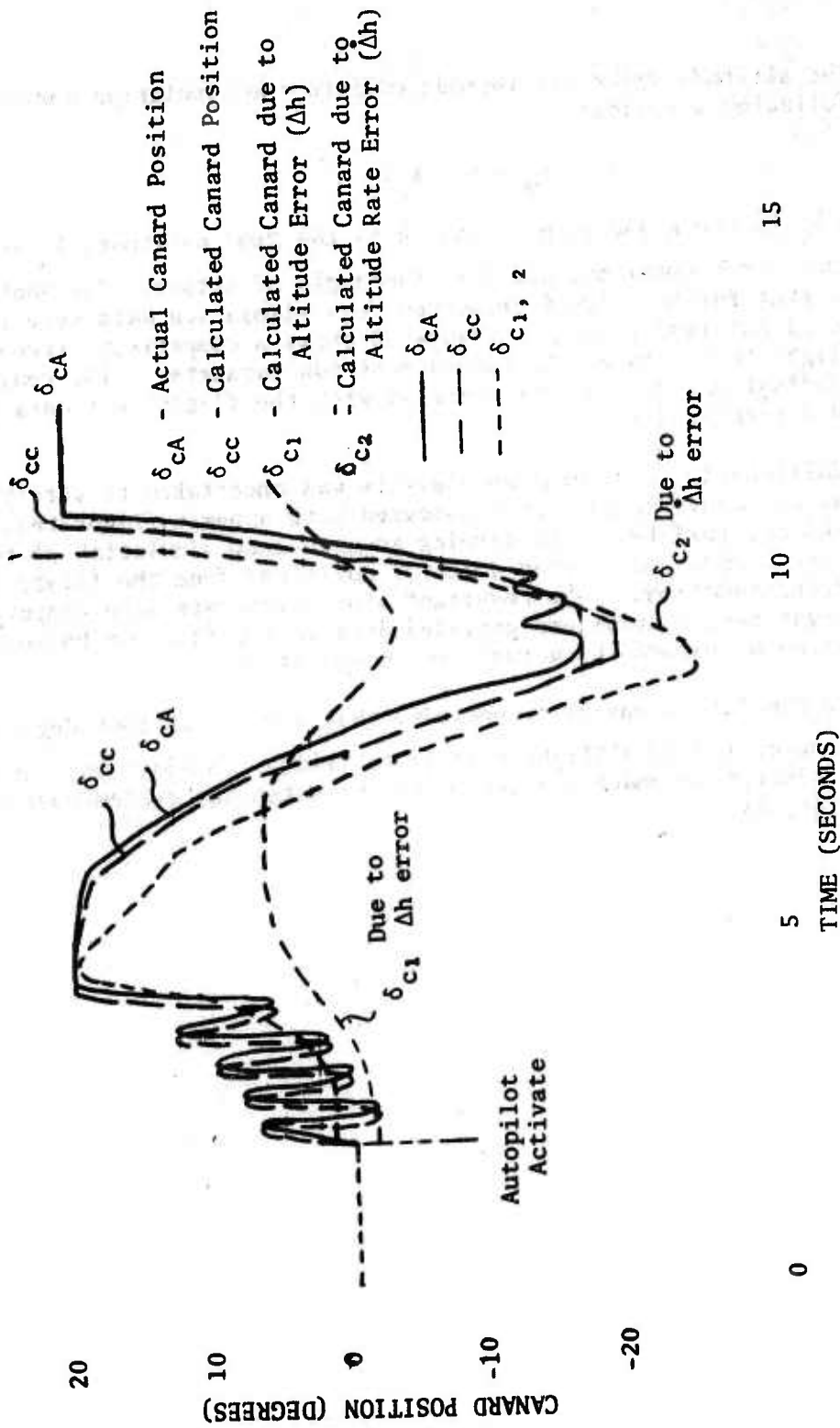


Figure 26. Calculated and Actual Canard Position vs Time

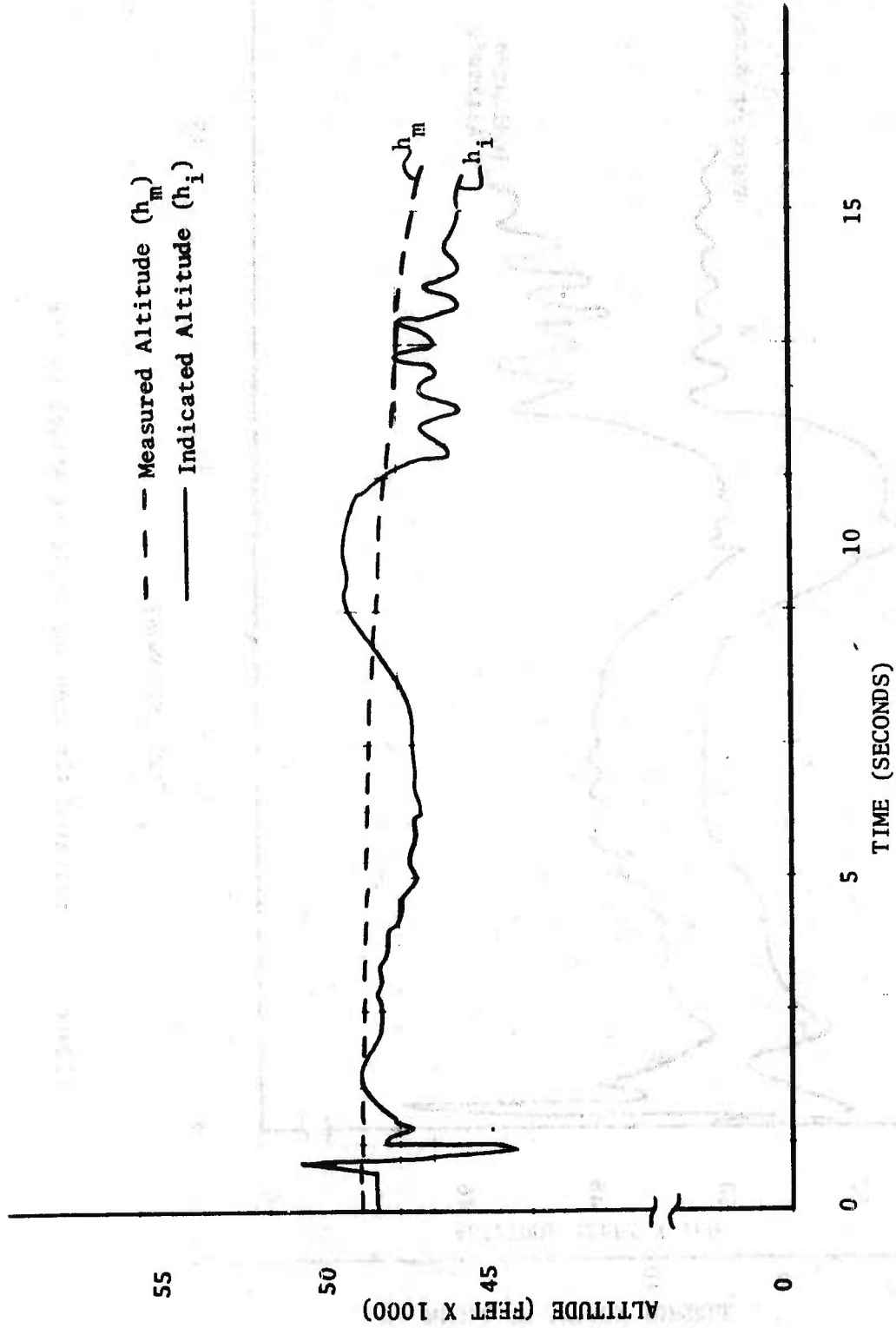


Figure 27. Measured and Indicated Altitude vs Time

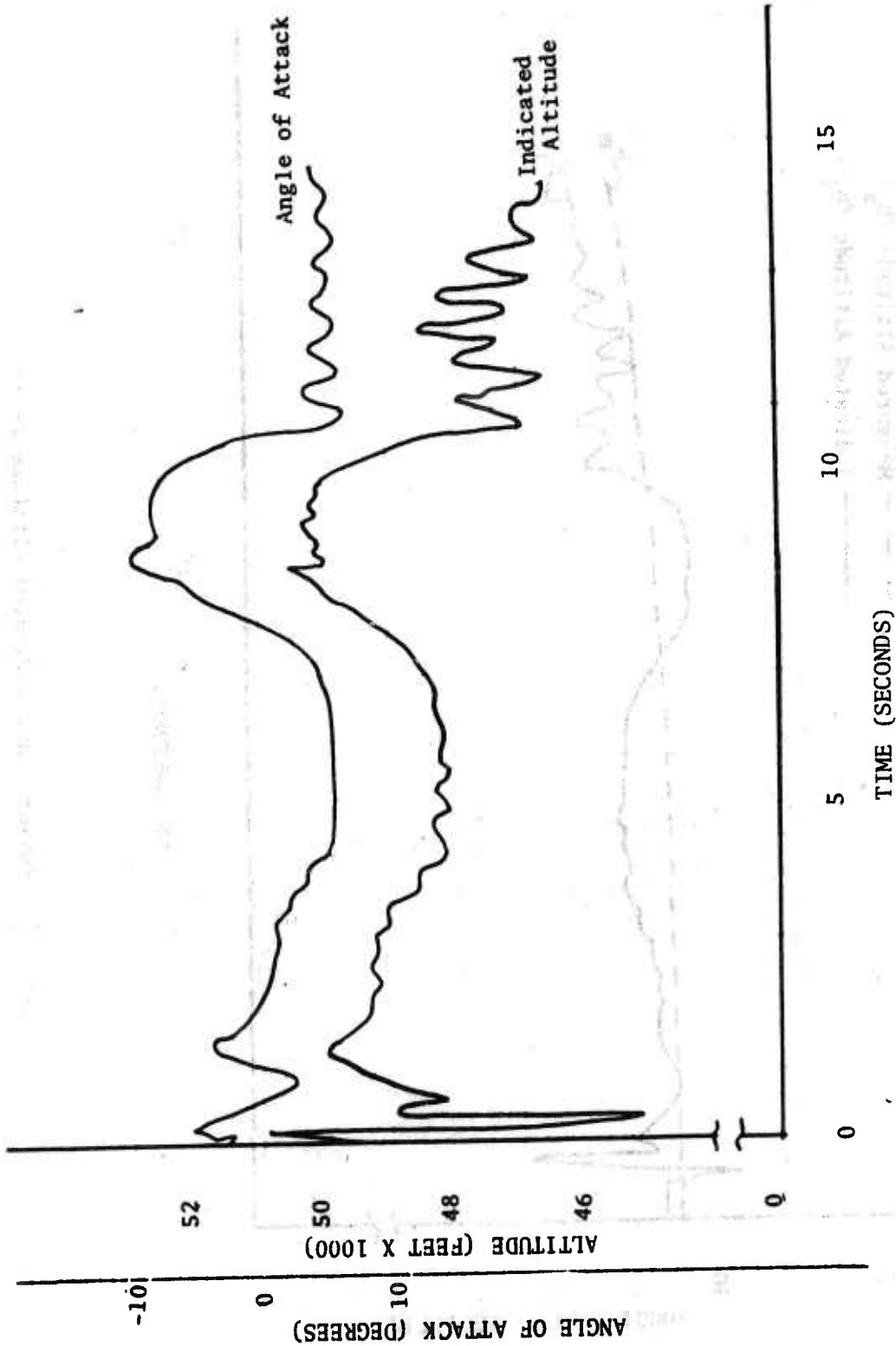


Figure 28. Indicated Altitude and Angle of Attack vs Time

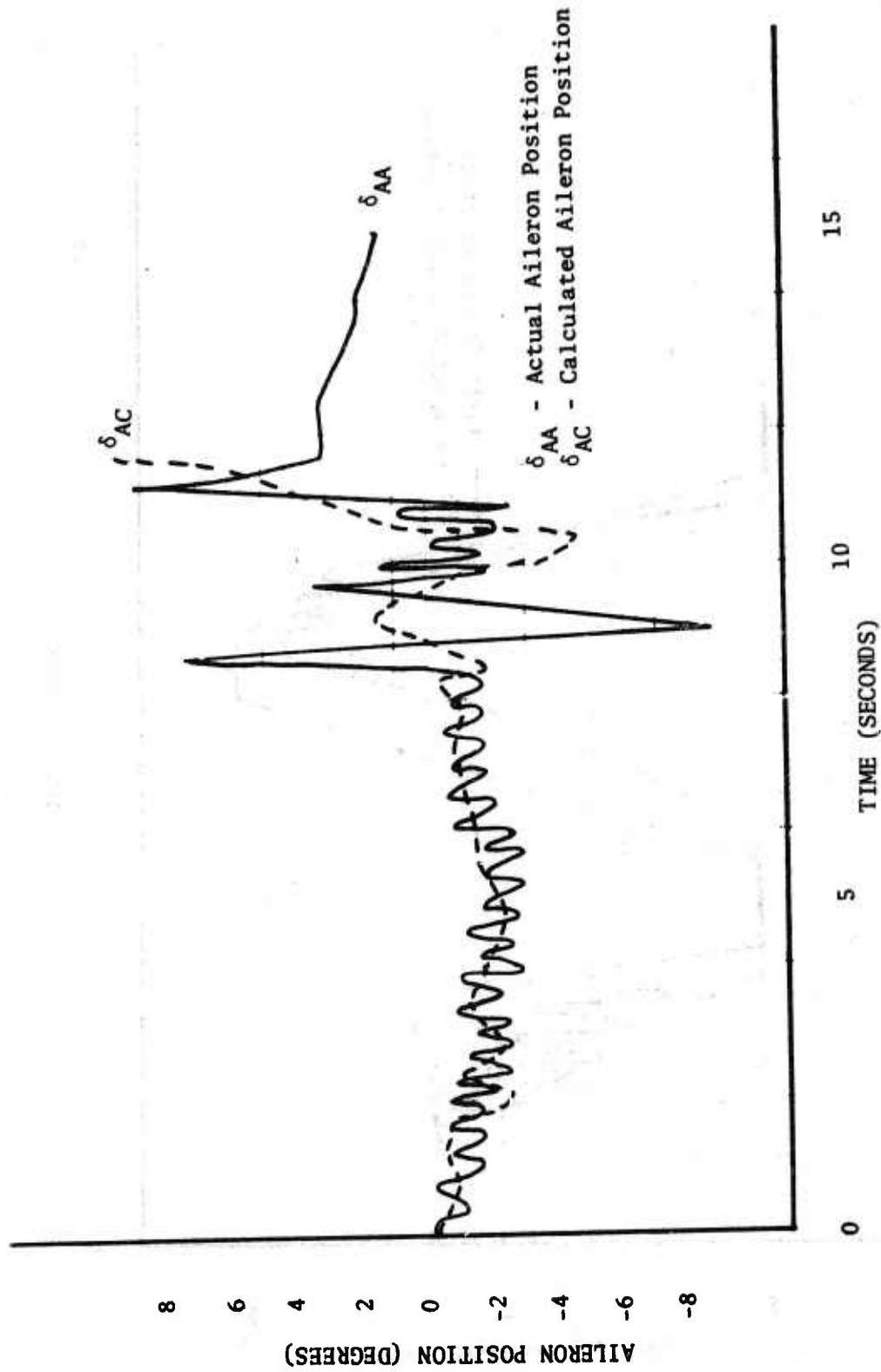


Figure 29. Calculated and Actual Aileron Position vs Time

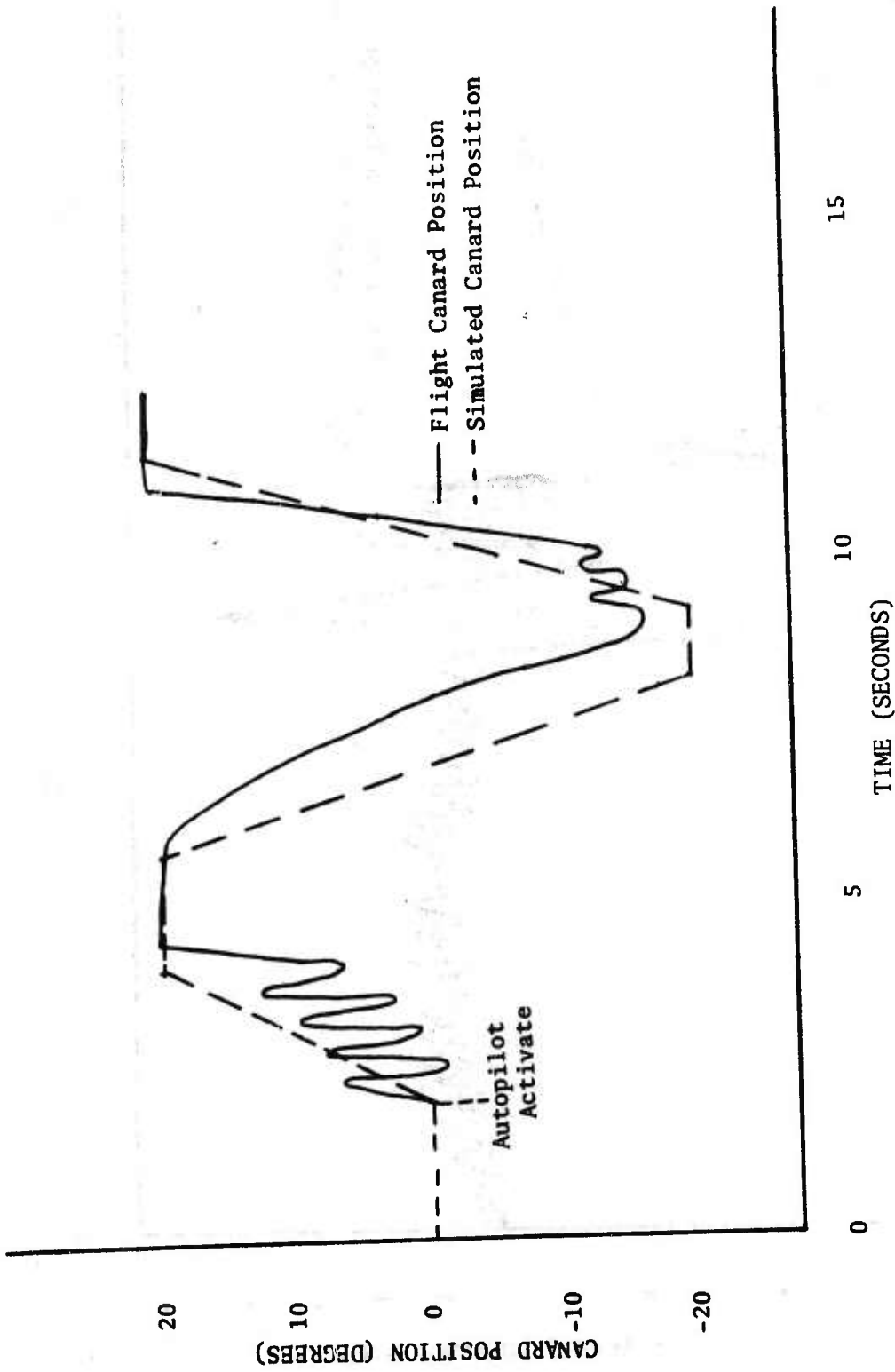


Figure 30. Flight and Simulated Canard Position vs Time

SECTION V

SYSTEM IMPROVEMENTS

A detailed stability and simulation analysis was performed on the system autopilot mechanization and altitude error. The results of this analysis determined that the following system improvements would be required: minimization of altitude error, alternate autopilot mechanization, and investigation of velocity control autopilot.

The analysis results showed that an altitude error of 10 feet/degree would be within the current guidance and control performance capabilities. However, this requires a 10 to 1 improvement in the altitude sensor and is beyond the hardware performance capabilities. Projected improvements to the pitot static tube could slightly reduce the error magnitude and reshape the characteristics so that the altitude error would provide overdamping; however, this would result in sluggish and unacceptable system performance.

Since the error is a function of the angle of attack, a measured angle-of-attack correction would compensate for the altitude error. This is not realizable, primarily due to packaging constraints and angle-of-attack hardware accuracy. A derived angle of attack could be achieved by using canard position and signal shaping. A comparison of canard position and angle of attack is presented in Figure 31. The derived angle of attack could also be obtained by use of the pitch rate gyro and the normal accelerometer in solving the following equations:

$$\theta = \alpha + \gamma, \quad \theta = \int \dot{\theta}, \quad \gamma = \frac{1}{V} \int N_z \quad (2)$$

Where θ is the integral of the pitch rate gyro, α is the angle-of-attack, γ is the flight path angle, V is the missile velocity, and N_z is the normal accelerometer. It should also be noted that the altitude measurements are a function of dynamic pressure. Therefore, for optimum compensation of the altitude error, a multi-function compensation derived from dynamic pressure and angle-of-attack measurements is required.

The use of a nose probe for sensing altitude would result in better sensor performance and greatly reduce the angle-of-attack sensitivity. Wind tunnel tests and analysis, to date, postulate an altitude error of 30 feet/degree, which is still beyond the current guidance and control performance capabilities but represents significant improvement. Additional compensation, as discussed previously, would further reduce the error magnitude; however, this approach affects the vector miss distance scoring system and the on-board radar augmentation. Tests have been planned to evaluate these effects extensively, but at present, the data available are insufficient for a decision on this method.

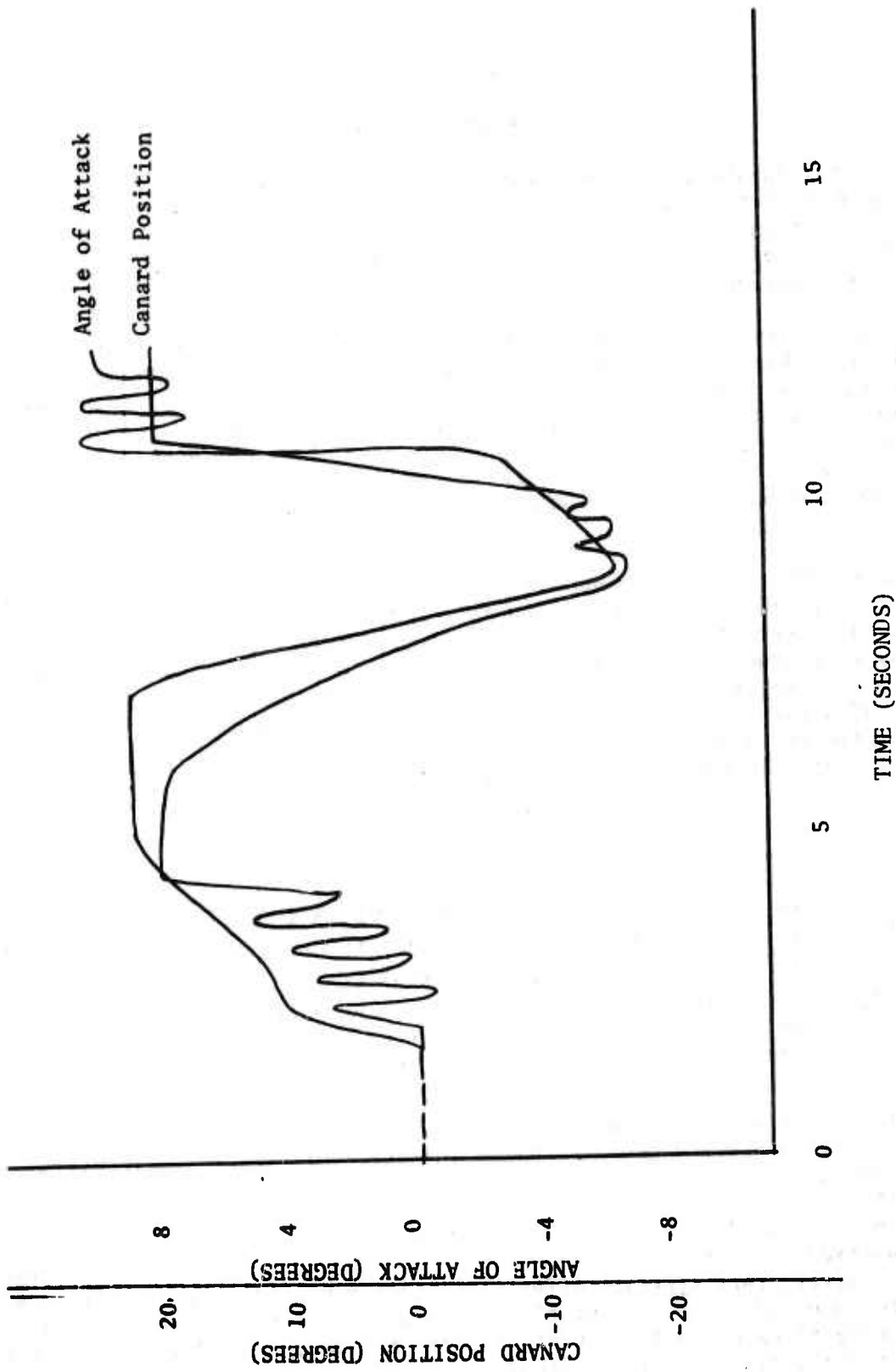


Figure 31. Angle of Attack and Canard Position vs Time

The techniques just discussed are methods of reducing the altitude sensor error and must be evaluated according to error magnitude and system performance. Extensive wind tunnel and analytical studies are currently in progress to define the error and performance improvements achievable throughout the performance envelope. Contingent on the results obtained, the best candidate approach for minimizing altitude error will be defined.

The present longitudinal autopilot mechanization can operate only in the presence of very small altitude errors because of the nature of its functional operation. Currently, the altitude rate is obtained by taking the derivative of the altitude measurement. This results in taking the derivative of the altitude error and introducing it into the more responsive altitude rate damping loop. This mechanization is marginal, at best, and should be replaced by an alternate approach. The following paragraphs discuss various alternate autopilot mechanizations, which increase in complexity and performance capability.

The easiest alternate mechanization would be to use the integral of the on-board accelerometer to provide altitude rate damping, in lieu of the derived rate. A stability and simulation analysis determined that this approach could maintain stable flight for altitude errors of 400 feet/degree at the dynamic pressure flight conditions around the KJ-4 flight case. At higher altitudes and large dynamic flight conditions, the performance decreased, as would be expected for a fixed gain autopilot mechanization, since it is compromised to achieve overall system performance. Applying signal shaping techniques to this mechanization allows for altitude errors of 600 feet/degree and improved transient response. Figures 32 and 33 are the overall root locus plots for the uncompensated and compensated versions of the previously discussed mechanizations and show the increased gain and phase margin of the compensated system.

The use of pitch attitude to provide altitude rate damping is another mechanization. This mechanization is less responsive and, accordingly, can tolerate a larger altitude error. The system is less responsive since it is providing rate damping by controlling on pitch attitude. Furthermore, this approach is compounded by the requirement for a quality attitude sensor. This sensor must have small corresponding drift rates to be compatible with missile flight times and accuracy requirements. The present dense system packaging does not readily permit installation of the additional sensor. Sensor cost is also a significant consideration.

Another mechanization that also uses the accelerometer would modify the original guidance equation to:

$$h_m = \frac{1}{2} (h - K_\alpha \alpha + \iint N_z) \quad (3)$$

X OPEN LOOP POLE

⊖ OPEN LOOP ZERO

Δ CLOSED LOOP $K_{\Delta h}$ DYNAMIC GAIN

▲ $K_{\Delta h} = 0.00005$ OPERATING GAIN

$$\text{GAIN MARGIN} = \frac{2.3 \times 10^{-4}}{0.5 \times 10^{-4}} > 4$$

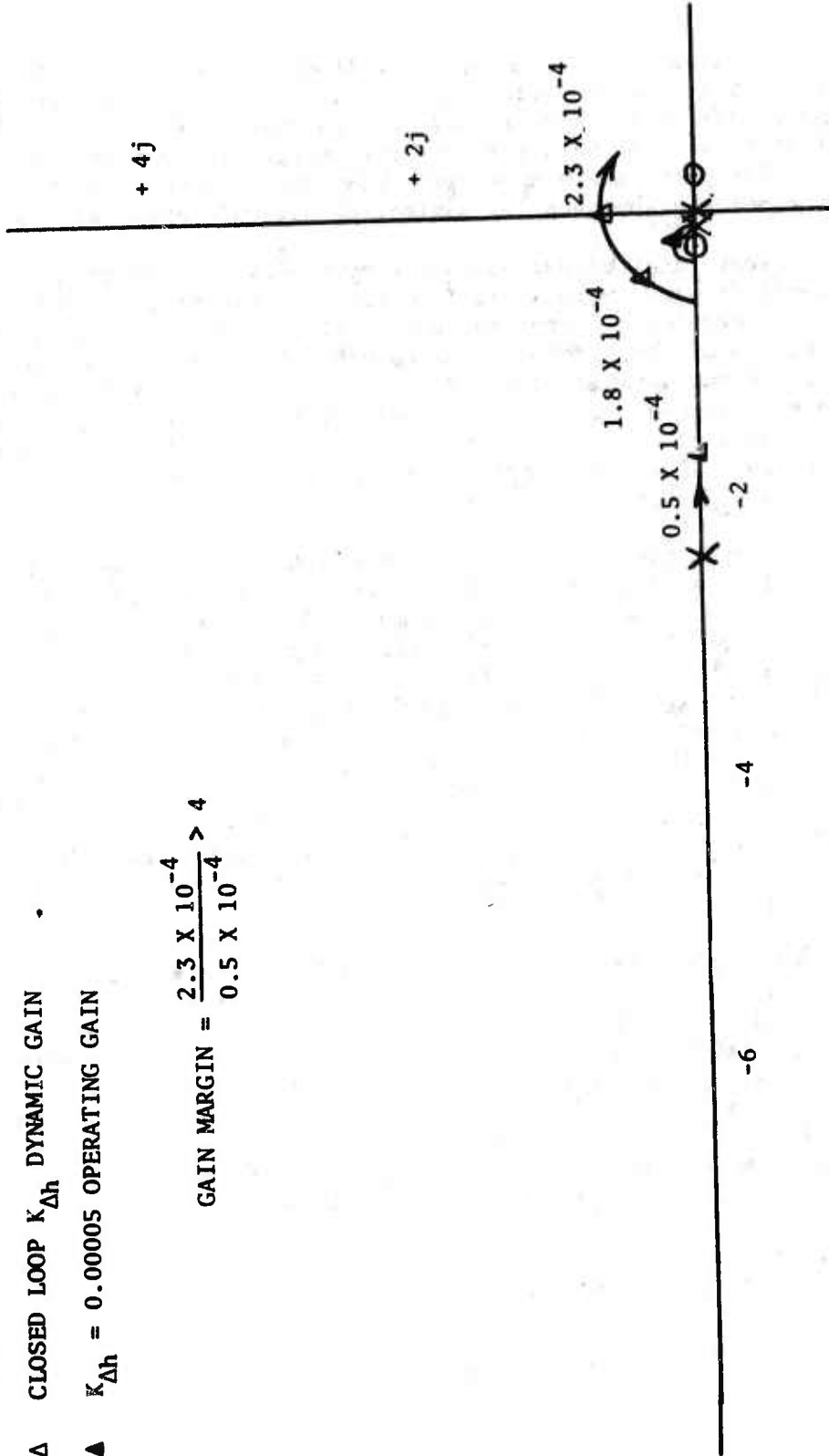


Figure 32. Altitude Loop (h/h_c), Integral of Acceleration Mechanization - Case 1. Root Locus Plot

X OPEN LOOP POLE

○ OPEN LOOP ZERO

△ CLOSED LOOP $K_{\Delta h}$ DYNAMIC GAIN

▲ $K_{\Delta h} = 0.125 \times 10^{-4}$ OPERATING GAIN

$$\text{GAIN MARGIN} = \frac{0.125 \times 10^{-3}}{0.125 \times 10^{-4}} > 10$$

$$\text{COMPENSATION} = \left(\frac{s}{0.5 + 1} \right) - \left(\frac{s}{2 + 1} \right)$$

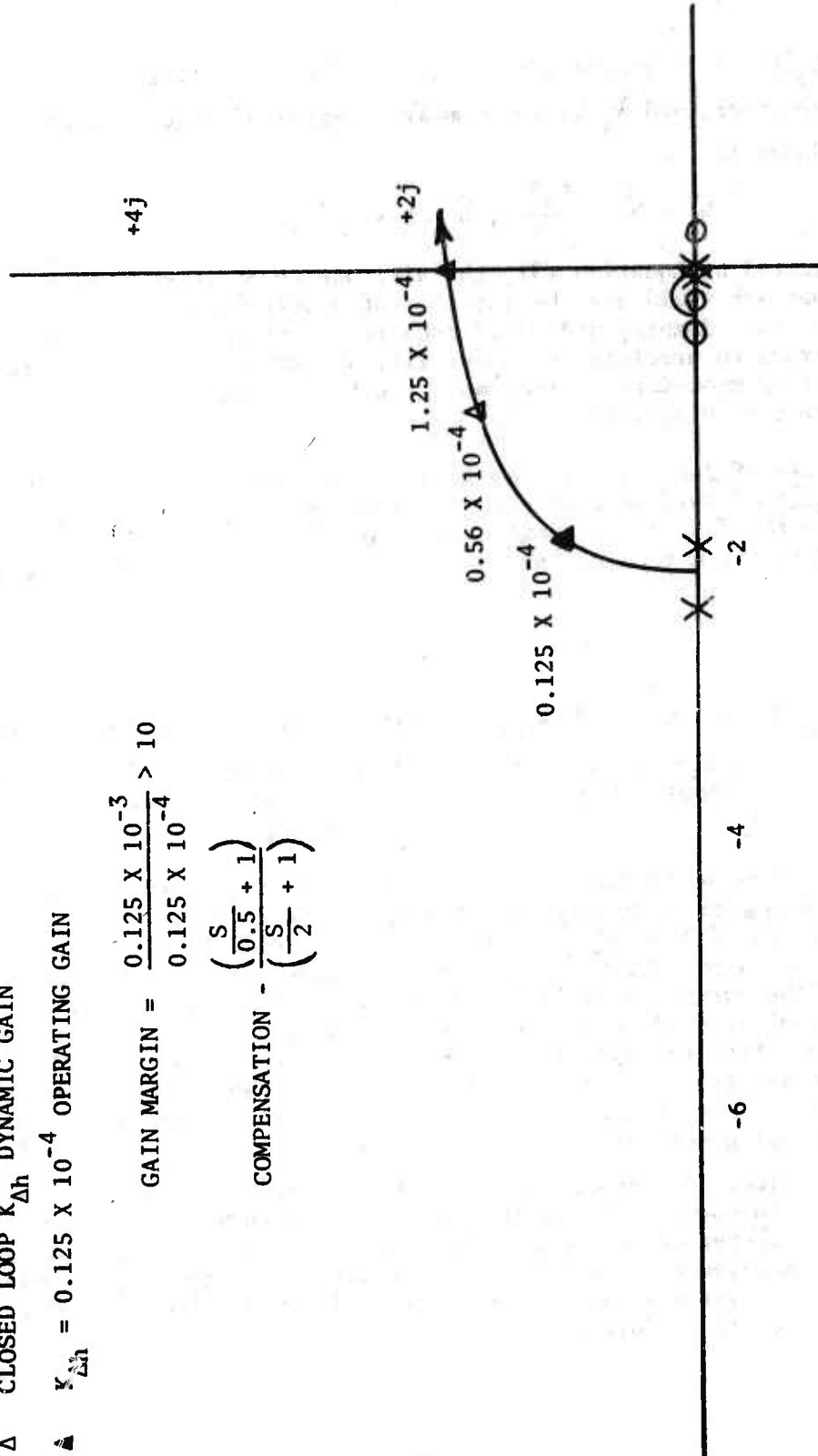


Figure 33. Altitude Loop (h/h_c),

Compensated Integral of Acceleration Mechanization - Case 1. Root Locus Plot

Where h_m is the measured altitude, h is the real altitude, $K_\alpha \alpha$ is the altitude error, and N_z is the double integral of acceleration. Equation (3) reduces to:

$$h_m = \hat{h} - \frac{K_\alpha \alpha}{2}, \quad \hat{h} = h + \iint N_z \quad (4)$$

As indicated by Equation (3), the altitude error is reduced by 50 percent. This approach would use the integral of accelerometer to provide system altitude rate damping and would require the minimization of accelerometer bias errors to preclude excessive altitude errors produced by the double integration procedure. Electronic signal shaping could also be used to minimize the integration errors.

The use of derived angle-of-attack compensation was discussed in the first part of this section when considering a reduction in the altitude error in the sensor implementation. However, this approach could also be applied to the autopilot through mechanization of the following guidance equation:

$$h_m = h - K_\alpha \alpha + K_{\alpha_d} \alpha_d \quad (5)$$

Where h_m , h , and $K_\alpha \alpha$ are as previously defined, and $K_{\alpha_d} \alpha_d$ is attitude error compensation as a function of derived angle-of-attack, for best results, K_{α_d} should also be a function of measured dynamic pressure.

The following autopilot mechanizations address overall improvements and concern signal shaping and an adaptive autopilot. In performing stability analysis studies of the present autopilot, the lack of signal shaping was apparent; this is especially true for the longitudinal autopilot. The current autopilot configuration is characterized as a fixed gain autopilot whose response varies considerably through the performance envelope. With the addition of properly chosen signal shaping, the dynamic system characteristics can be less sensitive throughout the performance envelope. The root locus plots shown in Figures 34 and 35 are of the longitudinal pitch rate loop ($\theta/\dot{\theta}_c$) shown in Figures 3 and 4, with signal shaping added. A comparison of these plots provides the results shown in Table 4. In summary, the addition of the compensation produces the following effects: increased frequency response and increased transient response. Similar improvements could be achieved with the remaining autopilot loops. The current system is stable, but the addition of signal shaping would improve overall performance.

- X OPEN LOOP POLE
- ⊖ OPEN LOOP ZERO
- Δ CLOSED LOOP K_q DYNAMIC GAIN
- ▲ $K_q = 0.02$ OPERATING GAIN

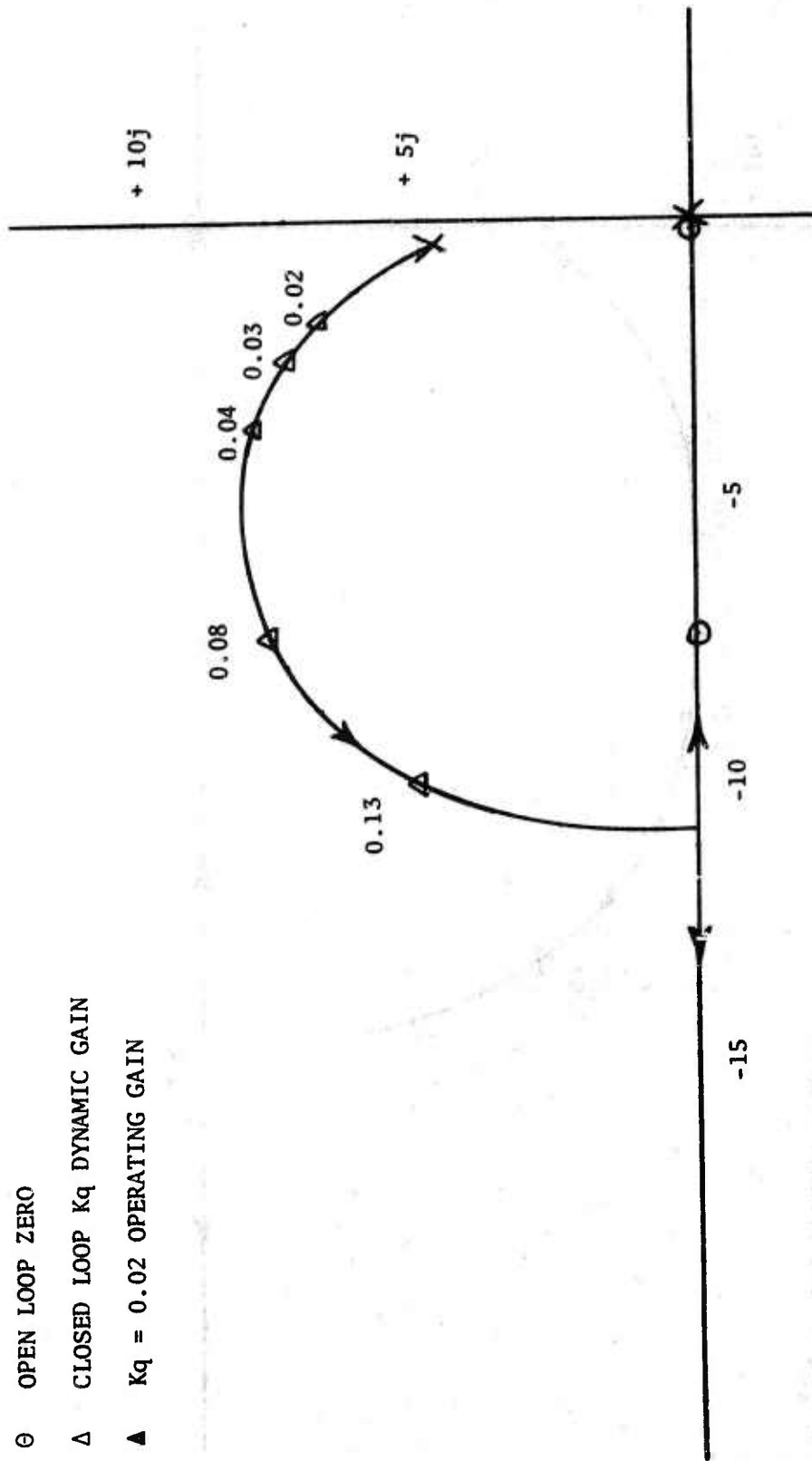


Figure 34. Compensated Rate Damping Loop ($\dot{\theta}/\dot{\theta}_c$) - Case 1. Root Locus Plot

X OPEN LOOP POLE

⊖ OPEN LOOP ZERO

Δ CLOSED LOOP K_q DYNAMIC GAIN

▲ $K_q = 0.02$ OPERATING GAIN

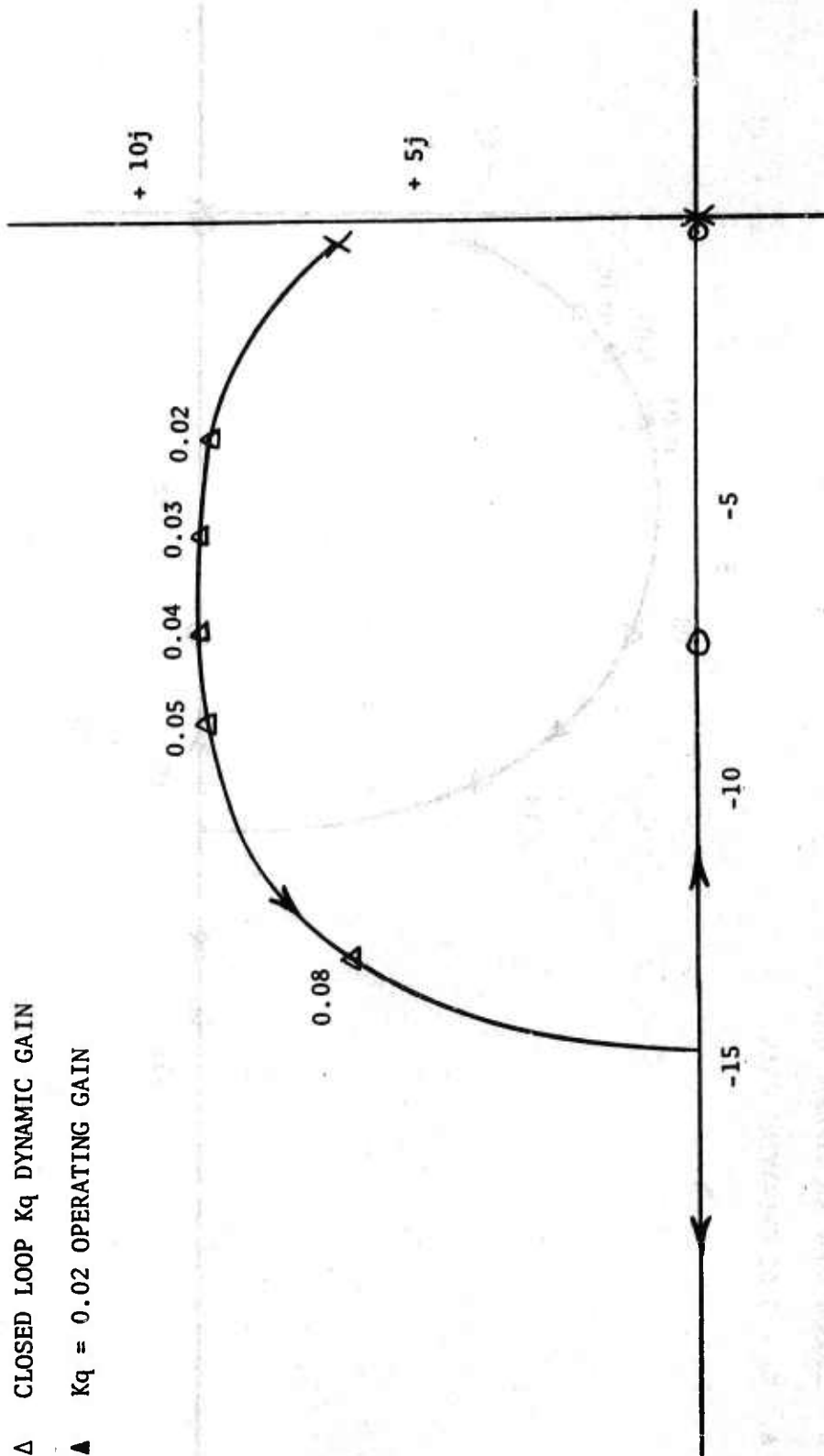


Figure 35. Compensated Rate Damping Loop ($\dot{\theta}/\dot{\theta}_c$) - Case 2. Root Locus Plot

TABLE 4. COMPARISON OF LONGITUDINAL AUTOPILOT
RATE DAMPING LOOP CHARACTERISTICS

<u>Analysis Cases</u>	<u>Uncompensated</u>		<u>Compensated</u>	
	ω_{η} (rad/sec)	a_{ξ}	ω_{η} (rad/sec)	a_{ξ}
Case 1.				
Nominal operating gain	2.5	1.0	7.5	0.15
+50%	2.0	1.0	8.0	0.20
+100%	1.5	1.0	9.0	0.27
Case 2.				
Nominal operating gain	2.5	1.0	9.5	0.26
+50%	2.0	1.0	11.0	0.35
+100%	1.8	1.0	12.0	0.44

a_{ξ} is the damping coefficient

The use of an adaptive or gain scheduling autopilot is a very attractive optimum mechanization and is readily achievable with the complement of guidance signals available. This autopilot would allow the system performance to operate around a nominal response by variation of autopilot gains. The autopilot gains would be a function of the following properly weighted signals: dynamic pressure, velocity, derived missile mass, derived moment of inertia, actuator position, and derived angle-of-attack. This would leave only the aerodynamic coefficients not measured, but these have less effect on the dynamics than those previously mentioned. However, if required, the aerodynamic coefficients could be derived from tables as a function of Mach and angle-of-attack. To exemplify the previous discussion, the following longitudinal dynamic transfer function equations will be used:

$$\Sigma M_y = I_y \ddot{\theta} = C_{m\alpha} \alpha q S D + C_{m\delta} \delta q S d + C_{m\dot{\theta}} \frac{\dot{\theta} q S d^2}{2V} + \quad (6)$$

$$C_{m\dot{\alpha}} \frac{\dot{\alpha} q S d}{2V} + C_{m\dot{\delta}} \frac{\dot{\delta} q S d}{2V}$$

$$\Sigma F = m V \dot{\gamma} = C_{N\alpha} \alpha q S + C_{N\delta} \delta q S \quad (7)$$

$$\theta = \alpha + \gamma \quad (8)$$

The individual parameters of the previous equations are determined accordingly:

S is missile reference area constant.

d is missile reference length constant.

q is measured dynamic pressure (air data module).

δ is measured actuator position (feedback potentiometer)

$\dot{\theta}$ is measured pitch rate (rate gyro).

V is measured missile velocity (air data module).

α is derived from δ or from $\alpha = \theta - \gamma$, $\theta = \int \dot{\theta}$, and $\gamma = (1/V) \int N_z$.

m is derived from integration of throttle valve position (feedback potentiometer).

N_z is measured normal acceleration (accelerometer).

I_y is a function of derived m .

The nominal aerodynamic coefficients could be used, and the small secondary terms (α , δ) could be neglected. Substitution of the previous parameters into Equations (6) to (8) allows solution of the dynamic equations throughout the flight envelope. These dynamic variations of the airframe, or autopilot control element, are defined within system tolerances, and the appropriate autopilot loop gains would be weighted to maintain a nominal performance bandwidth throughout the missile flight. This is attainable in a number of mechanization levels, and the benefits to be derived are worthwhile.

The velocity control autopilot is undergoing further investigation due to the indicated Mach number being sensitive to angle-of-attack variation. The Mach number is measured from the same pitot static tube as used for altitude, and similar errors are introduced into the velocity autopilot. A slight variation between measured and true Mach numbers were noted in the KJ-4 flight test results. These Mach number errors are small for low dynamic conditions but are significant at high dynamic conditions. Correction of the error could be achieved in the air data computer and have no impact on the current mechanization. The impact on the system will be defined from the results obtained in pitot static tube wind tunnel tests.

SECTION VI

CONCLUSION AND RECOMMENDATIONS

This guidance and control analysis of the HAST KJ-4 missile determined and parameterized the cause of the system flight test failure and proposes various system improvements for achieving required performance.

The cause of the present system instability is attributed to the system sensitivity to altitude errors introduced through the pitot static tube. These errors are a function of the missile angle of attack, and when they are coupled with the current autopilot configuration, the guidance and control performance capabilities are exceeded. Specifically, an altitude error of 100 feet/degree of angle of attack was experienced during the flight test, and a 10 foot/degree error can be handled by the present guidance and control system. This is beyond the system capabilities and warrants a combination of sensor improvement and an alternate autopilot mechanization.

As a secondary effect, the Mach number measurements derived from the same pitot static tube are also sensitive to the angle of attack. This presents no instability problem, and the significance is lessened with projected pitot static tube improvements.

Various system improvements are proposed for attaining the required system performance. Summarily, these trade-off error minimization in the sensor and candidate alternate autopilot mechanizations. Tables 5 and 6 summarize the improvement characteristics and list them according to increased complexity and performance capabilities. Currently, wind tunnel tests and related analytical studies are being performed to improve and to parameterize the pitot static tube performance. Following the analysis of the results obtained, the appropriate system configuration will be defined.

An additional worthwhile improvement to the system would be the use of signal shaping or an adaptive autopilot. Either of these would improve the overall system performance throughout the flight envelope by reducing the autopilot sensitivity to airframe dynamic variations. The recommended use of an adaptive autopilot is based on the number of readily available guidance signals and the large system dynamic variations.

TABLE 5. PITOT STATIC TUBE IMPROVEMENTS FOR MINIMIZING ALTITUDE ERRORS

<u>APPROACH</u>	<u>IMPLEMENTATION</u>	<u>EFFECTS</u>
Body probe	Improved static ports	No noticeable improvement
Body probe	Physical relocation & improved static ports	Same magnitude of error Overdamped system
Body probe	Angle-of-attack compensation in air data module 1. α calculated 2. α approximated	Significant improvement
Body probe	Angle-of-attack & dynamic pressure compensation in air data module	Optimum improvement Most complexity
Nose probe	Non-metallic or small metallic probe	Potential degradation of radar augmentation & vector miss indicator
Nose probe	Angle-of-attack & dynamic pressure compensation in air data module	Previous nose probe effects Potentially exceeds system requirements

TABLE 6. ALTERNATE AUTOPILOT MECHANIZATIONS FOR SYSTEM PERFORMANCE IMPROVEMENT^a

<u>APPROACH</u>	<u>IMPLEMENTATION</u>	<u>EFFECTS</u>
Integral of accelerometer	Integrate on-board accelerometer to provide altitude rate damping	Increased altitude error performance, $K_{\alpha} = 400$ ft/deg
Pitch attitude	Add pitch attitude gyro to provide attitude rate damping	Additional sensor & cost $K_{\alpha} = 800$ ft/deg Packaging constraints
Double integration of accelerometer	$h_m = \frac{1}{2}(h - K_{\alpha}\alpha + \iint N_z)$ and integral of accelerometer for altitude rate damping	Reduces K_{α} effect by 1/2 Double integration errors Minimized accelerometer bias errors required
Angle-of-attack	$h_m = h - K_{\alpha}\alpha + K_{\alpha d}d$ and integral of accelerometer for altitude rate damping	K_{α} effect reduced as accuracy of derived angle-of-attack α_d resolution
Signal shaping	Dynamic signal shaping of system response	Overall performance improvement Increases K_{α} tolerance
Adaptive or gain scheduling	Effective use of available guidance signals for achieving dynamic variations	Overall performance improvement Nominal performance throughout flight envelope

^aAs compared about KJ-4 dynamic conditions.

INITIAL DISTRIBUTION

ASD (ENYS)	3
AFFDL (FG)	1
Hq 4950 TESTW (TZHM)	1
AUL (AUL-LSE-70-239)	1
DDC	2
USAF (SAMI)	1
Ogden ALC (MMNOP)	2
AFWL (LR)	2
TRADOC (TAWC-LO)	1
AFATL (DL)	1
AFATL (DLB)	1
AFATL (DLM)	1
AFATL (DLMA)	7
AFATL (DLMH)	10
AFATL (DLMQ)	2
AFATL (DLOSL)	2
ADTC (XRC)	3